Dimolybdenum(III) Complexes of $-OSi(O^tBu)_3$, $-O_2P(O^tBu)_2$, and $-OB[OSi(O^tBu)_3]_2$ as Single-Source Molecular Precursors to Molybdenum-Containing, Multi-Component Oxide Materials

Kyle L. Fujdala and T. Don Tilley*

Department of Chemistry, University of California, Berkeley, Berkeley, California 94720-1460 and Chemical Sciences Division, Lawrence Berkeley National Laboratory, 1 Cyclotron Road, Berkeley, California 94720

Received July 10, 2003. Revised Manuscript Received January 15, 2004

The following dimolybdenum complexes containing $-OSi(O^tBu)_3$, $-O_2P(O^tBu)_2$, and $-OB[OSi(O^tBu)_3]_2$ ligands have been synthesized and structurally characterized: $Mo_2(NMe_2)_4[OSi(O^tBu)_3]_2$ (**1**), $Mo_2(O^tBu)_4[OSi(O^tBu)_3]_2$ (**2**), $Mo_2(NMe)_4\{OB[OSi(O^tBu)_3]_2\}_2$ (**3**), $Mo_2(NMe_2)_2[\mu\text{-}O_2P(O^tBu)_2]_2[O_2P(O^tBu)_2]_2$ (**4**), $Mo_2(NMe_2)_2[OSi(O^tBu)_3]_2[\mu\text{-}O_2P(O^tBu)_2]_2$ (**5**), and $Mo_2(NMe_2)_2[\mu\text{-}O_2P(O^tBu)_2]_2\{OB[OSi(O^tBu)_3]_2\}_2$ (**6**). The isolation and structural characterization of trans- and cis-isomers of complexes **4** and **5** (**4a** and **4b**, **5a** and **5b**, respectively) are also reported. Studies of the thermal decompositions of the complexes (by thermogravimetric analysis and solution ^1H NMR spectroscopy) were performed. Xerogels with approximate compositions of $2MoO_{1.5}\cdot 2P_2O_5$ and $2MoO_{1.5}\cdot 2P_2O_5\cdot 2SiO_2$ were derived from **4a** and **5a** or **5b**, respectively, via solution thermolyses (toluene). The as-synthesized (and dried) xerogels contain one equiv of $HNMe_2$ per molybdenum center (by combustion analysis, IR spectroscopy, and thermogravimetric analysis), and these materials have high surface areas (up to 270 $m^2\ g^{-1}$). Upon calcination at 300 °C, the coordinated amines are lost and the surface areas are significantly reduced (to 40 $m^2\ g^{-1}$ and <5 $m^2\ g^{-1}$ for the materials derived from **4** and **5a** or **5b**, respectively). Solid-state ^{31}P MAS NMR spectroscopy suggests that the as-synthesized xerogels retain structural features of the starting molecular precursors, as indicated by the presence of resonances that correspond to both bridging and terminal $-O_2P(O^tBu)_2$ ligands. Upon calcination at 300 °C, the resonances for bridging $-O_2P(O^tBu)_2$ groups are replaced by those for PO_4^{3-}. The material derived from **4** exhibits low activity and poor selectivity for the oxidative dehydrogenation (ODH) of propane to propylene. Cothermolyses of **4** and $Bi[OSi(O^tBu)_3]_3$ resulted in formation of Bi/Mo/P/Si/O materials with improved performance for the ODH of propane.

Introduction

The development of new methodologies for the generation of advanced materials is an active area of materials science and engineering. New synthetic routes are expected to play an increasingly important role in the design and synthesis of materials with novel properties.[1] The synthesis of multicomponent oxides with complex stoichiometries is of particular interest, as these materials are useful as heterogeneous catalysts, catalyst supports, electronic materials, and refractory materials.[1,2] Many of these applications require that the materials in question are highly homogeneous (atomically well-mixed). Often, this requires formation of metastable structures and low-temperature synthetic methods. The sol−gel route is a widely used approach for the synthesis of oxide materials and typically involves the hydrolysis and condensation of one or more single-element precursors (often alkoxides) in polar media.[1,3] Although quite effective for the synthesis of mono-element oxides, this method is less effective for the synthesis of multicomponent oxide materials.[3] Thus, the development of alternate routes to complex oxides

* To whom correspondence should be addressed. Phone 510-642-8939. Fax 510-642-8940. E-mail: tdtilley@socrates.berkeley.edu.

(1) (a) Uhlmann, D. R., Ulrich, D. R., Eds. *Ultrastructure Processing of Advanced Materials*; Wiley-Interscience: New York, 1992. (b) Bruce, D. W., O'Hare, D., Eds. *Inorganic Materials*; Wiley: New York, 1992. (c) Narula, C. K. *Ceramic Precursor Technology and Its Applications*; Marcel Dekker: New York, 1995. (d) Mehrotra, R. C. *J. Non-Cryst. Solids* **1988**, *100*, 1. (e) Stein, A.; Keller, S. W.; Mallouk, T. E. *Science* **1993**, *259*, 1558. (f) Amabilino, D. B.; Stoddart, J. F. *Chem. Rev.* **1995**, *95*, 2725. (g) Bowes, C. L.; Ozin, G. A. *Adv. Mater.* **1996**, *8*, 13.

(2) (a) Jolivet, J.-P. *Metal Oxide Chemistry and Synthesis−From Solution to Solid State*; John Wiley & Sons Ltd.: Chichester, 2000. (b) Klabunde, K. J. *Nanoscale Materials in Chemistry*; John Wiley & Sons: New York, 2001. (c) Bowker, M. *The Basis and Applications of Heterogeneous Catalysis*; Oxford University Press: New York, 1998. (d) Warren, B. K., Oyama, S. T. *Heterogeneous Hydrocarbon Oxidation*; ACS Symposium Series 638; American Chemical Society: Washington, DC, 1996. (e) Hondett, B. K. *Heterogeneous Catalytic Oxidation*; John Wiley & Sons: Chichester, 2000.

(3) (a) Brinker, C. J.; Scherer, G. W. *Sol−Gel Science*; Academic Press: Boston, 1990. (b) Klein, L. C., Ed. *Sol−Gel Technology for Thin Films, Fibers, Preforms, Electronics, and Specialty Shapes*; Noyes: Park Ridge, NJ, 1988. (c) Brinker, C. J. *J. Non-Cryst. Solids* **1988**, *100*, 31. (d) Schmidt, H. *J. Non-Cryst. Solids* **1988**, *100*, 51. (d) Schubert, U.; Hüsing, N.; Lorenz, A. *Chem. Mater.* **1995**, *7*, 2010. (e) Corriu, R. J. P.; Leclercq, D. *Angew. Chem., Int. Ed. Engl.* **1996**, *35*, 1421. (f) Schubert, U. *J. Chem. Soc., Dalton Trans.* **1996**, 3343.

10.1021/cm030563k CCC: $27.50
Published on Web 02/20/2004

may lead to materials with improved homogeneity and potentially unique properties.[4] We have been investigating the structure and reactivity of complexes containing $-OSi(O^tBu)_3$,[5] $-O_2Si(O^tBu)_2$,[6] and $-O_2P(O^tBu)_2$[7] ligands, for use as single-source molecular precursors to homogeneous M/Si/O and M/P/O mixed-element oxides via the *thermolytic molecular precursor* (TMP) route.[5−10]

Although the TMP route has been firmly established as an efficient method for the preparation of homogeneous two-component oxides, its use for the preparation of more complicated (tri- and tetra-component) materials from a single-source is relatively unexplored because of the lack of appropriate precursor complexes. Toward this end, we have recently reported the incorporation of $-OSi(O^tBu)_3$ *and* $-O_2P(O^tBu)_2$ ligands into a single complex, $[(^tBuO)_3SiO]_2Al[\mu-O_2P(O^tBu)_2]_2Al(Me)OSi(O^tBu)_3$, and have demonstrated its use as an efficient single-source molecular precursor to silicoaluminophosphates (SAPOs).[9] We have also recently synthesized a new ligand precursor containing both boron and silicon, $HOB[OSi(O^tBu)_3]_2$, for use in the generation of complexes containing the $-OB[OSi(O^tBu)_3]_2$ ligand.[10]

Previously, we described the dinuclear complexes $Mo_2[O_2Si(O^tBu)_2]_3$ and $W_2(HNMe_2)_2[O_2Si(O^tBu)_2]_2[OSi(OH)(O^tBu)_2]_2$, which serve as efficient single-source molecular precursors to Mo/Si/O and W/Si/O materials, respectively.[6] Since the first isolation of a triply bonded Mo_2L_6 complex by Wilkinson et al. in 1971,[11] scores of reports describing the preparation and reactivity of dimolybdenum(III) complexes have appeared, largely from the laboratories of Chisholm and Cotton.[12−16] Given the many applications of molybdenum-based materials as oxidation catalysts,[2c,d,e,17] most of which are oxides containing three or more elemental components, we have extended the TMP procedures utilized previously for the generation of more complex structures involving molybdenum. Many molybdenum-based oxide catalysts are prepared from polyoxomolybdates.[18,19] Alternative molecular sources of molybdenum containing several additional elements, for use in TMP methods, could lead to the discovery of materials with novel catalytic properties. Herein, we report the syntheses and structural characterizations of several new triply bonded dimolybdenum(III) complexes containing various combinations of $-OSi(O^tBu)_3$, $-O_2P(O^tBu)_2$, and $-OB[OSi(O^tBu)_3]_2$ ligands. The thermal decompositions of these complexes have been investigated, and they have been employed as molecular precursors to multicomponent oxide materials. The oxidative dehydrogenation of propane to propylene was investigated using Mo/P/O and Mo/Bi/Si/P/O materials derived from these molecular precursors.

Results and Discussion

Synthesis and Characterization of Precursor Complexes. The reaction of 2 equivs of $HOSi(O^tBu)_3$ with $Mo_2(NMe_2)_6$ in pentane afforded $Mo_2(NMe_2)_4[OSi(O^tBu)_3]_2$ (**1**; eq 1). Analytically pure yellow crystals of **1** were isolated in 76% yield from pentane at −78 °C. In an analogous fashion, the reaction of 2 equiv of $HOSi(O^tBu)_3$ with $Mo_2(O^tBu)_6$ in pentane, followed by crystallization from pentane at −30 °C, afforded analytically pure $Mo_2(O^tBu)_4[OSi(O^tBu)_3]_2$ (**2**) as red crystals in 59%

(4) For examples of "non-hydrolytic sol−gel methods" see (a) Jansen, M.; Guenther, E. *Chem. Mater.* **1995**, *7*, 2110. (b) Vioux, A. *Chem. Mater.* **1997**, *9*, 2292.

(5) For selected recent examples see: (a) Terry, K. W.; Lugmair, C. G.; Gantzel, P. K.; Tilley, T. D. *Chem. Mater.* **1996**, *8*, 274. (b) Su, K.; Tilley, T. D.; Sailor, M. J. *J. Am. Chem. Soc.* **1996**, *118*, 3459. (c) Terry, K. W.; Lugmair, C. G.; Tilley, T. D. *J. Am. Chem. Soc.* **1997**, *119*, 9745. (d) Terry, K. W.; Su, K.; Tilley, T. D.; Rheingold, A. L. *Polyhedron* **1998**, *17*, 891. (e) Kriesel, J. W.; Tilley, T. D. *J. Mater. Chem.* **2001**, *11*, 1081. (f) Fujdala, K. L.; Tilley, T. D. *Chem. Mater.* **2001**, *13*, 1817. (g) Lugmair, C. G.; Fujdala, K. L.; Tilley, T. D. *Chem. Mater.* **2002**, *14*, 888. (h) Fujdala, K. L.; Tilley, T. D. *Chem. Mater.* **2002**, *14*, 1376.

(6) Su, K.; Tilley, T. D. *Chem. Mater.* **1997**, *9*, 588.

(7) (a) Lugmair, C. G.; Tilley, T. D.; Rheingold, A. L. *Chem. Mater.* **1997**, *9*, 339. (b) Lugmair, C. G.; Tilley, T. D. *Inorg. Chem.* **1998**, *37*, 1821. (c) Lugmair, C. G.; Tilley, T. D. *Inorg. Chem.* **1998**, *37*, 6304. (d) Lugmair, C. G.; Tilley, T. D.; Rheingold, A. L. *Chem. Mater.* **1994**, *6*, 1615.

(8) (a) Kriesel, J. W.; Sander, M. S.; Tilley, T. D. *Mater. Chem.* **2001**, *13*, 3554. (b) Kriesel, J. W.; Sander, M. S.; Tilley, T. D. *Adv. Mater.* **2001**, *13*, 331.

(9) Fujdala, K. L.; Tilley, T. D. *J. Am. Chem. Soc.* **2001**, *123*, 10133.

(10) Fujdala, K. L.; Olliver, A. G.; Hollander, F. J.; Tilley, T. D. *Inorg. Chem.* **2003**, *42*, 1140.

(11) Huq, F.; Mowat, W.; Shortland, A.; Skapski, A. C.; Wilkinson, G. *Chem. Commun.* **1971**, 1079.

(12) (a) Chisholm, M. H.; Cotton, F. A. *Acc. Chem. Res.* **1978**, *11*, 356. (b) Chisholm, M. H.; Cotton, F. A.; Frenz, B. A.; Reichert, W. W.; Shive, L. W.; Stults, B. R. *J. Am. Chem. Soc.* **1976**, *98*, 4469. (c) Chisholm, M. H.; Cotton, F. A.; Murillo, C. A.; Reichert, W. W. *Inorg, Chem.* **1977**, *16*, 1801. (d) Chisholm, M. H.; Cotton, F. A.; Extine, M. W.; Reichert, W. W. *J. Am. Chem. Soc.* **1978**, *100*, 153. (e) Chisholm, M. H.; Rothwell, I. P. *J. Am. Chem. Soc.* **1980**, *102*, 5950. (f) Chetcuti, M. J.; Chisholm, M. H.; Folting, K.; Haitko, D. A.; Huffman, J. C.; Janos, J. *J. Am. Chem. Soc.* **1983**, *105*, 1163.

(13) (a) Chisholm, M. H.; Cotton, F. A.; Extine, M. W.; Reichert, W. W. *J. Am. Chem. Soc.* **1978**, *100*, 1727. (b) Chisholm, M. H.; Haitko, D. A.; Huffman, J. C.; Folting, K. *Inorg. Chem.* **1981**, *20*, 2211. (c) Chisholm, M. H.; Folting, K.; Huffman, J. C.; Rothwell, I. P. *Inorg. Chem.* **1981**, *20*, 2215. (d) Chisholm, M. H.; Huffman, J. C.; Kirkpatrick, C. C. *Inorg. Chem.* **1983**, *22*, 1704. (e) Chetcuti, M. J.; Chisholn, M. H.; Folting, K.; Haitko, D. A.; Huffman, J. C. *J. Am. Chem. Soc.* **1982**, *104*, 2138. (f) Chisholm, M. H.; Cotton, F. A.; Folting, K.; Huffman, J. C.; Ratermann, A. L.; Shamshoum, E. S. *Inorg. Chem.* **1984**, *23*, 4423. (g) Cotton, F. A.; Su, J.; Yao, Z. *Inorg. Chim. Acta* **1997**, *266*, 65.

(14) (a) Chisholm, M. H.; Haitko, D. A.; Huffman, J. C.; Folting, K. *Inorg. Chem.* **1981**, *20*, 171. (b) Chisholm, M. H.; Folting, K.; Huffman, J. C.; Rothwell, I. P. *Inorg. Chem.* **1981**, *20*, 1496. (c) Chisholm, M. H.; Huang, J.-H.; Huffman, J. C.; Parkin, I. P. *Inorg. Chem.* **1997**, *36*, 1642. (d) Chisholm, M. H.; Folting, K.; Hoffman, J. C.; Li, H.; Macintosh, A. M.; Wu, D.-D. *Polyhedron* **2000**, *19*, 375.

(15) (a) Coffindaffer, T. W.; Rothwell, I. P.; Huffman, J. C. *Inorg. Chem.* **1983**, *22*, 2907. (b) Coffindaffer, T. W.; Rothwell, I. P.; Huffman, J. C. *Inorg. Chem.* **1984**, *23*, 1433.

(16) (a) Bursten, B. E.; Cotton, F. A.; Green, J. C.; Seddon, E. A.; Stanley, G. G. *J. Am. Chem. Soc.* **1980**, *102*, 4579. (b) Dobbs, K. D.; Francl, M. M.; Hehre, W. J. *Inorg. Chem.* **1984**, *23*, 24. (c) Liu, X.-Y.; Alvarez, S. *Inorg. Chem.* **1997**, *36*, 1055. (d) Chisholm, M. H.; Macintosh, A. M.; Huffman, J. C.; Wu, D.; Davidson, E. R.; Clark, R. J. H.; Firth, S. *Inorg. Chem.* **2000**, *39*, 3544. (e) Chisholm, M. C.; Davidson, E. R.; Huffman, J. C.; Quinlan, K. B. *J. Am. Chem. Soc.* **2001**, *123*, 9652.

(17) (a) Liu, H. F.; Liu, R. S.; Liew, K. Y.; Johnson, R. E.; Lunsford, J. H. *J. Am. Chem. Soc.* **1984**, *106*, 4117. (b) Zhen, K. J.; Khan, M. M.; Mak, C. H.; Lewis, K. B.; Somorjai, G. A. *J. Catal.* **1985**, *94*, 501. (c) Suzuki, K.; Hayakawa, T.; Shimizu, M.; Takehira, K. *Catal. Lett.* **1995**, *30*, 159. (d) Ruth, K.; Kieffer, R.; Burch, R. *J. Catal.* **1998**, *175*, 16. (e) Ruth, K.; Burch, R.; Kieffer, R. *J. Catal.* **1998**, *175*, 27. (f) Costentin, G.; Savary, L.; Lavalley, J. C.; Borel, M. M.; Grandin, A. *Chem. Mater.* **1998**, *10*, 59. (g) Lin, M.; Desai, T. B.; Kaiser, F. W.; Klugherz, P. D. *Catal. Today* **2000**, *61*, 223. (h) Sherrington, D. C. *Catal. Today* **2000**, *57*, 87. (i) Imamura, S.; Sasaki, H.; Shono, M.; Kanai, H. *J. Catal.* **1998**, *177*, 72. (j) Neumann, R.; LevinElad, M. *J. Catal.* **1997**, *166*, 206. (k) Juwiler, D.; Blum, J.; Neumann, R. *Chem. Commun.* **1998**, 1123. (k) Arnold, U.; Serpa da Cruz, R.; Mandelli, D.; Schuchardt, U. *J. Mol. Catal. A* **2001**, *165*, 149. (l) Yuan, S.; Hamid, S. B. D.-A.; Li, Y.; Ying, P.; Xin, Q.; Derouane, E. G.; Li, C. *J. Mol. Catal. A* **2002**, *180*, 245. (m) Dallmann, K.; Buffon, R.; Loh, W. *J. Mol. Catal. A* **2002**, *178*, 43.

(18) (a) Chen, Q.; Zubieta, J. *Coord. Chem. Rev.* **1992**, *114*, 107. (b) Baker, L. C. W.; Glick, D. C. *Chem. Rev.* **1998**, *98*, 3. (c) Jeannin, Y. P. *Chem. Rev.* **1998**, *98*, 51. (d) Gouzerh, P.; Proust, A. *Chem. Rev.* **1998**, *98*, 77. (e) Klemperer, W. G.; Wall, C. G. *Chem. Rev.* **1998**, *98*, 297. (f) Katsoulis, D. E. *Chem. Rev.* **1998**, *98*, 359.

(19) (a) Kozhevnikov, I. V. *Chem. Rev.* **1998**, *98*, 171. (b) Mizuno, N.; Makoto, M. *Chem. Rev.* **1998**, *98*, 199.

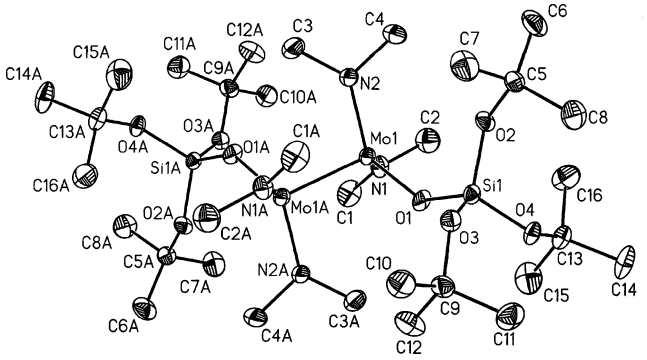

Figure 1. Thermal ellipsoid plot of **1** at the 50% probability level. Hydrogen atoms have been omitted for clarity.

yield (eq 2). Complexes **1** and **2** are soluble in nonpolar solvents and both are oxygen- and moisture-sensitive. The ^{1}H NMR spectrum of **1** indicates the presence of two conformations in a 1:4 ratio. Two major (broad) resonances (in a 1:1 ratio) centered at 4.42 and 2.75 ppm and two minor sharp resonances (in a 1:1 ratio) at 4.17 and 2.80 ppm are attributed to the N−Me groups. The low field resonances (∼4 ppm) correspond to proximal methyl groups, directed over the Mo−Mo bond, for each of the two conformations, and the high-field resonances (∼2.8 ppm) correspond to distal methyl groups located away from the Mo−Mo bond.[12] The large magnetic anisotropy associated with the Mo−Mo triple bond is the primary reason for the downfield shift of the proximal methyl groups.[12b] Two sharp resonances at 1.50 (minor) and 1.49 (major) attributed to the −OSi(O^{t}Bu)$_3$ groups for the two conformations are also observed in a 1:4 ratio. Analogously, multiple conformations have been previously observed in the solution ^{1}H NMR spectrum (low-temperature) of $Mo_2(NMeEt)_6$ and other related Mo_2(III) species.[12] The solid-state structure of **1** exhibits distinct proximal and distal N−Me groups with the −OSi(O^{t}Bu)$_3$ ligands arranged in a staggered manner; this is likely the major structure in solution (Figure 1). Only one set of resonances is observed in the ^{1}H NMR spectrum of complex **2** (1.61 ppm for the Mo−O^{t}Bu groups and 1.49 ppm for the Si−O^{t}Bu groups), and the solid-state structure of **2** shows that the −OSi(O^{t}Bu)$_3$ groups are also arranged in a staggered fashion (Figure 2).

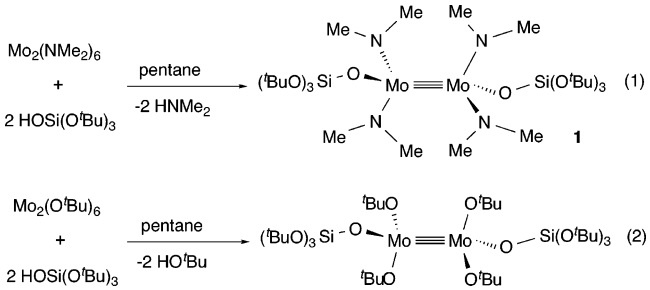

Crystallographic data and selected bond distances and angles for **1** and **2** are provided in the Supporting Information. The Mo−Mo distances in **1** and **2** (2.2098(5) and 2.2464(7) Å, respectively) are within the normal range of distances observed for triply bonded Mo−Mo species (2.17 to 2.30 Å).[12a,16c] The Mo−O(Si) distances of 1.961(2) and 1.931(2) for **1** and **2**, respectively, are significantly longer than the Mo−O(C) distances in **2** (1.863(2) and 1.887(2)), indicating greater π-donation for the *tert*-butoxide ligands versus the tris(*tert*-butoxy)siloxide ligands.

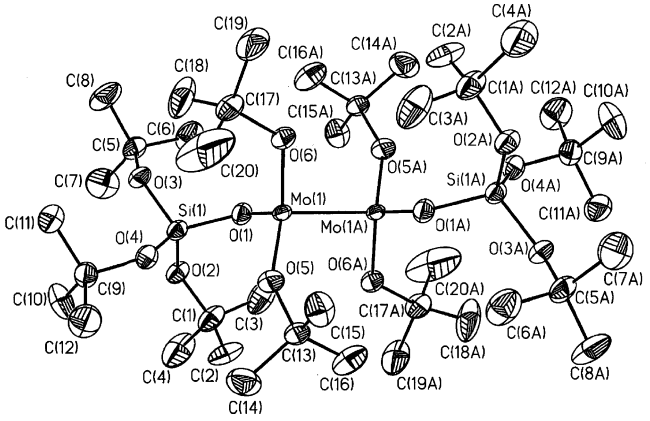

Figure 2. Thermal ellipsoid plot of **2** at the 50% probability level. Hydrogen atoms have been omitted for clarity.

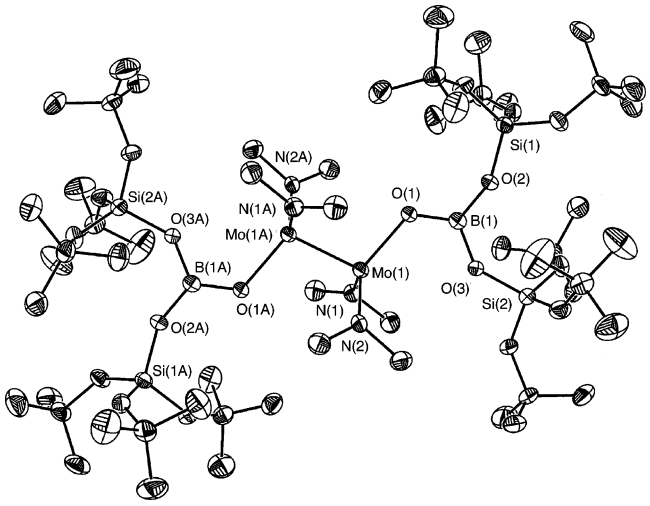

Figure 3. Thermal ellipsoid plot of **3** at the 50% probability level. Hydrogen atoms have been omitted for clarity.

Reaction of 2 equivs of HOB[OSi(O^{t}Bu)$_3$]$_2$ with Mo_2(NMe$_2$)$_6$ in pentane afforded Mo_2(NMe)$_4${OB[OSi(O^{t}Bu)$_3$]$_2$}$_2$ (**3**; eq 3). Analytically pure yellow crystals of **3** were obtained via crystallization from a pentane solution at −30 °C (73% yield). The ^{1}H NMR spectrum of **3** reveals one conformation, containing proximal and distal N−Me groups. The observation of only one conformation is reasonable given the large steric bulk of the −OB[OSi(O^{t}Bu)$_3$]$_2$ ligand, which enforces a staggered conformation to maximize the distance between ligands. Indeed, this structure is reflected in the solid state (Figure 3). Complex **3** is a rare example of a transition metal boryloxide complex and is the second such species containing the −OB[OSi(O^{t}Bu)$_3$]$_2$ ligand, the other being Cp$_2$Zr(Me)OB[OSi(O^{t}Bu)$_3$]$_2$ (Cp = cyclopentadienyl).[10] Chisholm et al. have previously isolated and structurally characterized the related triply

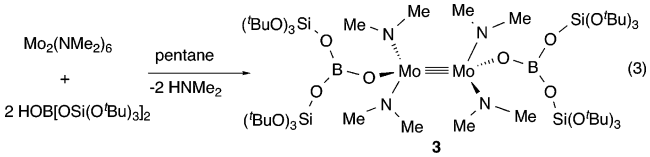

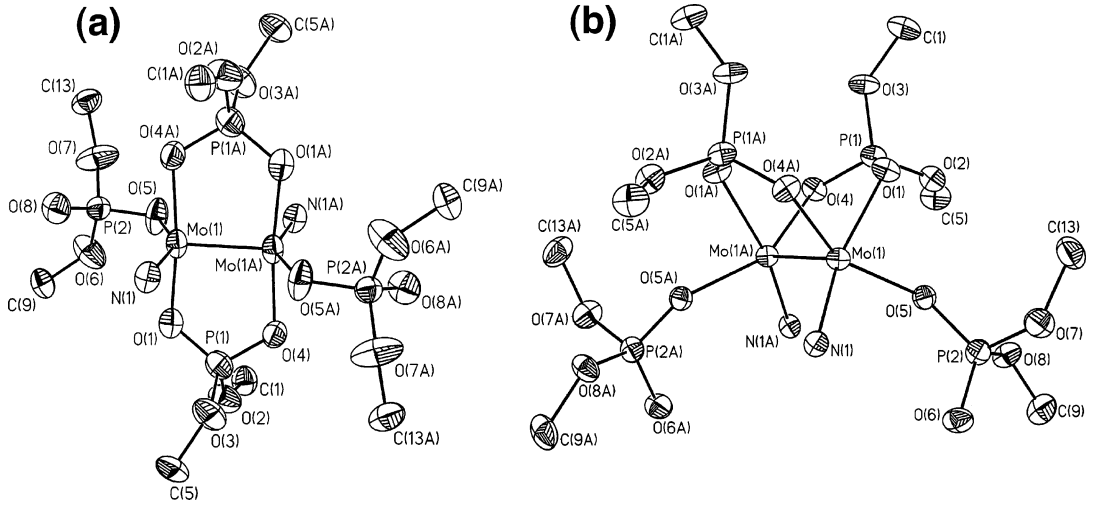

Figure 4. Thermal ellipsoid plots of (a) **4a** and (b) **4b** at the 50% probability level. Solvate molecules, hydrogen atoms, and methyl groups have been omitted for clarity.

bonded ditungsten diarylboryloxides $W_2(NMe_2)_4(OBMes_2)_2$ and $W_2(O^tBu)_4(OBMes_2)_2$ (Mes = 2,4,6-trimethylphenyl),[20] and Gibson and co-workers have reported the synthesis of $Mo_2(NMe_2)_4(OBMes_2)_2$.[21]

Crystallographic data and selected bond distances and angles for **3** are given in the Supporting Information. The Mo−Mo bond distance (2.2107(9) Å) is within the normal range for triply bonded Mo_2(III) species.[12a,16c] The relatively long Mo−O(B) distance (2.005(2) Å) suggests less π-donation from the $-OB[OSi(O^tBu)_3]_2$ group to the metal versus the alkoxide and siloxide ligands (see **1** and **2** above).[15] The boron atoms in **3** are in a trigonal planar environment, as indicated by the sum of the O−B−O angles (359.9(4)°). The Mo−O−B angle of 121.8(2)° is considerably smaller than the terminal $M-O-BAr_2$ angles in the previously reported transition metal diarylboryloxides, which range from 141(1) to 168.4(5)°.[20,22]

In an attempt to substitute the NMe_2 ligands for O^tBu groups in **3**, the reaction of 4 equiv of ^{t}BuOH with **3** was examined. This reaction results in replacement of the NMe_2 ligands with $-O^tBu$ groups; however, transfer of one siloxide group from B to Mo is also observed as indicated by the isolation of **2** as the only major product (as red crystals in 55% yield). A similar $-OSi(O^tBu)_3$ transfer has been previously observed in the conversion of $Cp_2Zr(Me)OB[OSi(O^tBu)_3]_2$ to $Cp_2Zr[OSi(O^tBu)_3]_2$ upon thermolysis.[11] Reactions of **3** with HO^iPr and EtOH do not lead to the formation of isolable species, and several products are observed (by ^{1}H NMR spectroscopy). Additionally, reaction of $HOB[OSi(O^tBu)_3]_2$ with $Mo_2(O^tBu)_6$ leads only to isolation of **2**, again with $-OSi(O^tBu)_3$ transfer from B to Mo. Although the fate of all of the boron in these transformations is unknown, resonances corresponding to small amounts of ^{t}BuOB$[OSi(O^tBu)_3]_2$[11] are observed in the ^{1}H NMR spectra of reaction mixtures for both the ^{t}BuOH + **3** and $HOB[OSi(O^tBu)_3]_2$ + $Mo_2(O^tBu)_6$ reactions, suggesting that transfer of $-O^tBu$ groups to boron has occurred.

Reaction of 4 equiv of $HOP(O)(O^tBu)_2$ with $Mo_2(NMe_2)_6$ in pentane produced the trans isomer (vide supra) of $Mo_2(NMe_2)_2[\mu\text{-}O_2P(O^tBu)_2]_2[O_2P(O^tBu)_2]_2$ (**4a**) in 74% isolated yield as orange crystals (eq 4). The identification of **4a** as the trans isomer is provided by a solid-state structure analysis (Figure 4a). A very small amount (<5%) of the yellow cis isomer of $Mo_2(NMe_2)_2[\mu\text{-}O_2P(O^tBu)_2]_2[O_2P(O^tBu)_2]_2$ (**4b**, Figure 4b) was obtained after prolonged storage of solutions of **4** at −30 °C. The reaction of 4 equiv of $HOP(O)(O^tBu)_2$ with $Mo_2(NMe_2)_6$ in benzene-d_6 at 25 °C led to the exclusive formation of **4a** (by ^{1}H NMR spectroscopy). The ^{1}H NMR spectrum of **4a** consists of sharp resonances at 5.32 and 3.05 ppm attributed to the N−Me groups, and resonances at 1.65 and 1.50 ppm for the two types of $P(O^tBu)$ groups (bridging and terminal). The ^{1}H NMR spectrum of **4b** in benzene-d_6 contains sharp resonances at 5.05 and 3.27 ppm for the N−Me groups, and resonances at 1.71, 1.66, 1.47, and 1.46 ppm for the two types of $-O_2P(O^tBu)_2$ groups (bridging and terminal), each with inequivalent ^{t}Bu groups. The ^{31}P NMR spectrum of **4a** contains two sharp resonances at 22.43 and −6.90 ppm corresponding to the bridging and terminal $-O_2P(O^tBu)_2$ groups, respectively, and the ^{31}P NMR spectrum of **4b** exhibits resonances with similar chemical shifts (24.42 and −6.14 ppm). Reactions of 2 equiv of ROH (R = ^{t}Bu, ^{i}Pr, and Et) with **4a** in benzene-d_6 did not lead to substitution of the NMe_2 groups (no reaction). In fact, complex **4a** appears to be moderately air- and moisture-stable, exhibiting signs of decomposition only after several days of exposure to the atmosphere.

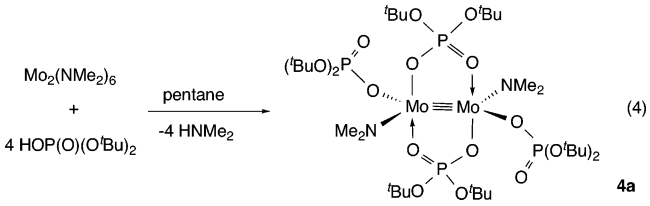

(4)

The crystallographic details and bond distances and angles for **4a** and **4b** are summarized in the Supporting Information. The presence of both bridging and terminal $-O_2P(O^tBu)_2$ ligands in the isomers of $Mo_2(NMe_2)_2[\mu$-

(20) Chisholm, M. H.; Folting, K.; Haubrich, S. T.; Martin, J. D. *Inorg. Chim. Acta* **1993**, *213*, 17.
(21) Gibson, V. C.; Redshaw, C.; Clegg, W.; Elsegood, M. R. J. *Polyhedron* **1997**, *16*, 2637.
(22) Chen, H.; Power, P. P.; Shoner, S. C. *Inorg. Chem.* **1990**, *30*, 2884.

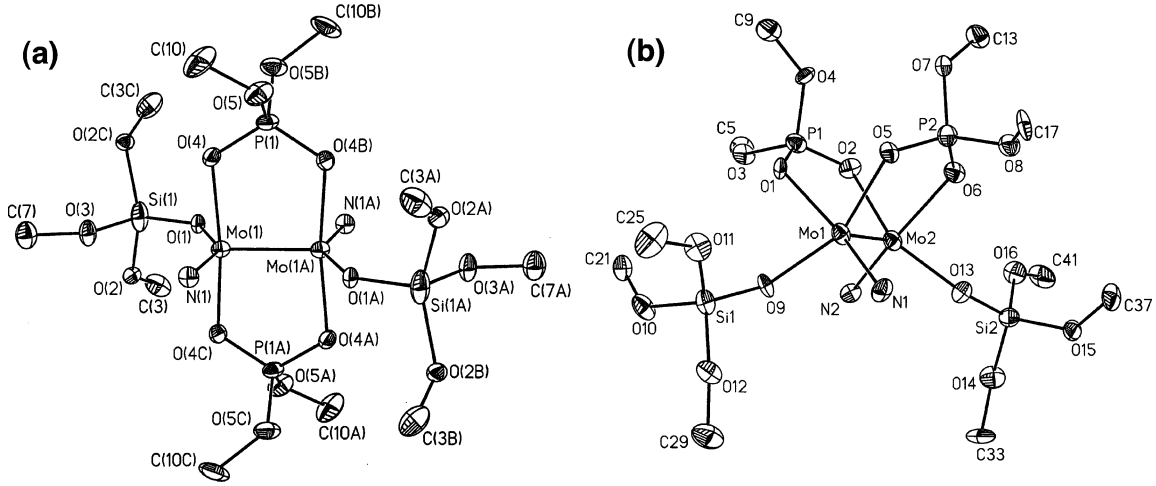

Figure 5. Thermal ellipsoid plots of (a) **5a** and (b) **5b** at the 50% probability level. Solvate molecules, hydrogen atoms, and methyl groups have been omitted for clarity.

$O_2P(O^tBu)_2]_2[O_2P(O^tBu)_2]_2$ is consistent with the ability of phosphate and phosphonate ligands to exhibit multiple coordination modes.[7,23] The Mo−Mo distances in **4a** and **4b** (2.2335(9) and 2.2171(6) Å, respectively) are within the normal range for such bonds.[12a,16c] The molybdenum centers in **4a** are in a distorted trigonal bipyramidal environment, whereas the coordination geometry of the molybdenum atoms in **4b** is a distorted square pyramid (Figure 4).

Numerous investigations have addressed the diversity of structures for triply bonded dimolybdenum species,[12−16] but few containing two bridging ligands have been structurally characterized.[13,14d,15b] These complexes generally exhibit a geometry with the two bridging ligands in a mutually cis arrangement; however, $W_2(O^tBu)_4$-$[N(C_6H_5)C(O)O^tBu]_2$ exhibits a trans disposition of the bridging ligands.[13f] Thus, the observation of trans and cis isomers of $Mo_2(NMe_2)_2[\mu\text{-}O_2P(O^tBu)_2]_2[O_2P(O^tBu)_2]_2$ (**4a** and **4b**, respectively) is somewhat unusual. For a doubly bridged, quadruply bonded dimolybdenum complex, $Mo_2(O_2CCMe_3)_2Cl_2(PEt_3)_2$, cis and trans isomers have been structurally characterized.[24] For other quadruply bonded dimolybdenum complexes containing two bridging ligands, either cis[25] or trans[26] geometries have been observed.

The reaction of 2 equiv of $HOP(O)(O^tBu)_2$ with **1** in pentane led to the formation of significant amounts of both the trans and cis isomers (vide supra) of $Mo_2(NMe_2)_2[OSi(O^tBu)_3]_2[\mu\text{-}O_2P(O^tBu)_2]_2$ (**5a** and **5b**, respectively; eq 5). Cooling the reaction mixture to −78 °C led to isolation of analytically and spectroscopically pure red crystals of the less soluble trans isomer (**5a**) in 38% yield. Concentration of the mother liquor and cooling to −78 °C provided yellow crystals of **5b** in 23% yield. Dissolution of **5a** or **5b** in benzene-d_6 does not lead to interconversion at room temperature, or at 80 °C (30 min). The ^{31}P NMR spectra of **5a** and **5b** each exhibit only one resonance (at 22.95 and 20.97 ppm, respectively), attributed to the bridging $-O_2P(O^tBu)_2$ ligand. Thus, both complexes exist in a single conformation.

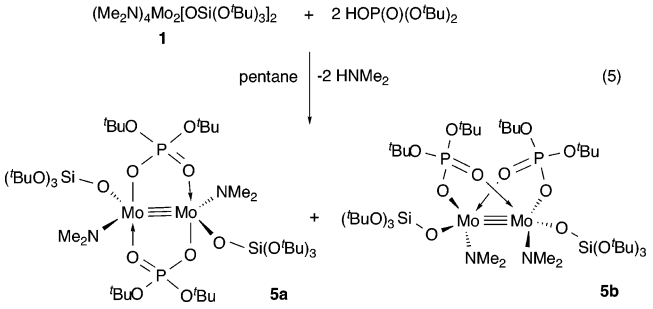

X-ray structural characterizations reveal that **5a** and **5b** are the trans and cis isomers of $Mo_2(NMe_2)_2[OSi(O^tBu)_3]_2[\mu\text{-}O_2P(O^tBu)_2]_2$, respectively (Figure 5a and b; Supporting Information). The Mo−Mo distances for **5a** and **5b** (2.236(1) and 2.245(2) Å, respectively) are within the normal range for triply bonded Mo−Mo species.[12a,16c] In contrast to **4a**, the Mo−O(P) linkages in **5a** (2.105(3) Å) are equivalent (crystallographically imposed). Complexes **5a** and **5b** represent the first transition metal compounds containing both the $-O_2P(O^tBu)_2$ *and* $-OSi(O^tBu)_3$ ligands.[9] The formation of significant amounts of both the trans and cis isomers of **5** (**5a** and **5b**, respectively) may arise from the trapping of the two conformations of **1** that are present in solution (see discussion above). As observed for **4a** and **4b**, the geometries of the Mo centers in **5a** are in a distorted trigonal bipyramidal environment, whereas the molybdenum atoms in **5b** have a distorted square pyramidal coordination geometry.

The reaction of 2 equiv of $HOP(O)(O^tBu)_2$ with **3** in pentane provided purple crystals of *trans*-$Mo_2(NMe_2)_2$-

(23) For leading references see: (a) Walawalkar, M. G.; Roesky, H. W.; Murugavel, R. *Acc. Chem. Res.* **1999**, *32*, 117. (b) Murugavel, R.; Sathiyendiran, M.; Walawalkar, M. G. *Inorg. Chem.* **2001**, *40*, 427. (c) Chakraborty, D.; Chandrasekhar, V.; Bhattacharjee, M.; Krätzner, R.; Roesky, H. W.; Noltemeyer, M.; Schmidt, H.-G. *Inorg. Chem.* **2000**, *39*, 23. (d) Guzyr, O. I.; Siefken, R.; Chakraborty, D.; Roesky, H. W.; Teichert, M. *Inorg. Chem.* **2000**, *39*, 1680. (e) Yin, L.; Cheng, P.; Yan, S.-P.; Fu, X.-Q.; Li, J.; Liao, D.-Z.; Jiang, Z.-H. *J. Chem. Soc., Dalton Trans.* **2001**, 1398. (f) Mason, M. *J. Cluster Sci.* **1998**, *9*, 1. (g) Thorn, D. L.; Harlow, R. L. *Inorg. Chem.* **1992**, *31*, 3917. (h) Chang, Y.-D.; Zubieta, J. *Inorg. Chem. Acta* **1996**, *245*, 177. (i) Küsthardt, U.; LaBarre, M. J.; Enemark, J. H. *Inorg. Chem.* **1990**, *29*, 3182.

(24) Arenivar, J. D.; Mainz, V. V.; Ruben, H.; Andersen, R. A.; Zalkin, A. *Inorg. Chem.* **1982**, *21*, 2649.

(25) (a) Agaskar, P.; Cotton, F. A. *Inorg. Chem. Acta* **1984**, *83*, 33. (b) Fanwick, P. E. *Inorg. Chem.* **1985**, *24*, 258. (c) Chen, J.-D.; Cotton, F. A.; Kang, S.-J. *Inorg. Chem. Acta* **1991**, *190*, 103. (d) Burk, J. H.; Whitwell II, G. E.; Lemley, J. T.; Burlitch, J. M. *Inorg. Chem.* **1983**, *22*, 1306. (e) Suen, M.-C.; Wu, Y.-Y.; Chen, J.-D.; Keng, T.-C.; Wang, J.-C. *Inorg. Chem. Acta* **1999**, *288*, 82.

(26) (a) Girolami, G. S.; Mainz, V. V.; Andersen, R. A. *J. Am. Chem. Soc.* **1982**, *104*, 2041. (b) Cotton, F. A.; Powell, G. L. *Polyhedron* **1985**, *4*, 1669. (c) Yu, S.-B. *Polyhedron* **1992**, *11*, 2115. (d) Wu, Y.-Y.; Chen, J.-D.; Liou, L.-S.; Wang, J.-C. *Inorg. Chem. Acta* **1997**, *258*, 193.

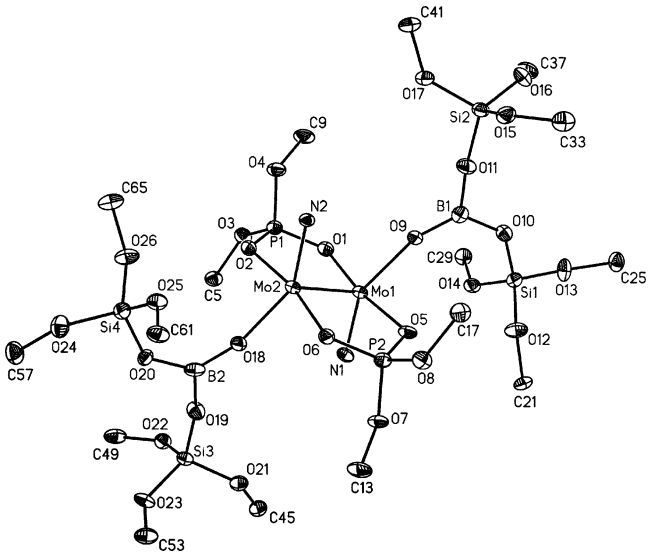

Figure 6. Thermal ellipsoid plot of **6** at the 50% probability level. Hydrogen atoms and methyl groups have been omitted for clarity.

$[\mu\text{-}O_2P(O^tBu)_2]_2\{OB[OSi(O^tBu)_3]_2\}_2$ (**6**) (22%, Figure 6) upon cooling the reaction mixture to −30 °C (eq 6). Observation of only the trans isomer of **6** may reflect the extreme steric demands of the $-OB[OSi(O^tBu)_3]_2$ ligand, which may prevent formation of what would be a more crowded cis isomer. The ^{1}H NMR spectrum of **6** reveals only one conformation in solution with sharp resonances at 5.78 and 3.17 ppm for the N−Me groups, and resonances at 1.57 and 1.56 ppm for the SiO^tBu and PO^tBu groups, respectively. The ^{31}P NMR spectrum of **6** exhibits one resonance at 21.02 ppm, consistent with the presence of one $\mu\text{-}O_2P(O^tBu)_2$ ligand.

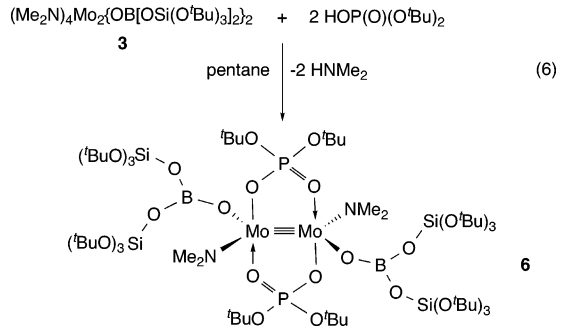

Selected metrical parameters and crystallographic data for **6** are given in the Supporting Information. The Mo−Mo distance in **6** (2.2505(5) Å) is similar to those in **1**−**5** and other triply bonded Mo_2 complexes.[12a,16c] The Mo−O(B) distances (2.027(3) and 2.022(3) Å) in **6** are similar to those observed for **3**. In contrast, the Mo−O−B angles in **6** (162.4(3) and 164.8(3)°) are much larger than the Mo−O−B angles in **3** (121.8(2)°).

Conversions of 2−6 to Oxide Materials. Thermogravimetric analysis (TGA) of **2** (N_2, 10 °C min^{-1}) reveals a precipitous weight loss at ∼100 °C and ceramic yields of 39.8% at 200 °C and 36.9% at 600 °C, in close agreement with the calculated ceramic yields for $2MoO_3\cdot 2SiO_2$ (40.4%) and $2MoO_{1.5}\cdot 2SiO_2$ (35.6%) (Figure 7). A second precipitous mass loss, attributed to sublimation of MoO_3, occurs at >700 °C. The ceramic yield at 1000 °C (10.9%) corresponds closely to that expected for $2SiO_2$

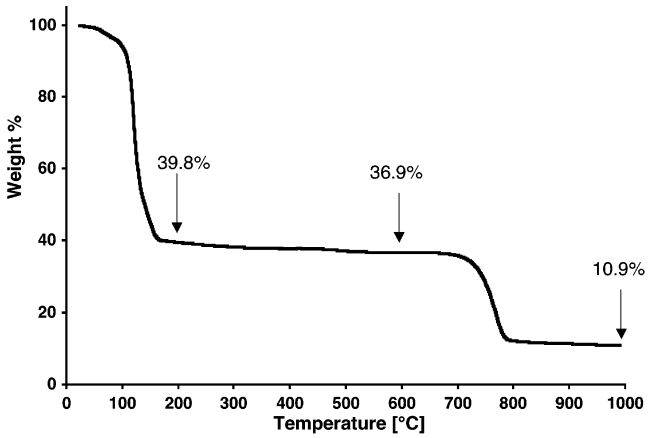

Figure 7. TGA trace of **2** under N_2 with a heating rate of 10 °C min^{-1}.

(11.9%) suggesting that all of the molybdenum sublimes away as MoO_3, as is commonly observed for Mo-containing oxide materials.[6,27] These TGA results indicate that complex **2** is an effective single-source molecular precursor to Mo/Si/O materials.[6]

Thermolysis of a benzene-d_6 solution of **3** at 150 °C resulted in formation of small amounts of CH_2CMe_2 along with several unidentifiable species containing $-O^tBu$ groups, as indicated by the presence of several broad resonances in the ^{1}H NMR spectrum of the reaction mixture. Prolonged heating at 150 °C did not lead to a significant change in the thermolysis mixture. The presence of soluble metal species after thermolysis suggests that **3** may not be ideal for use as a single-source molecular precursor via solution thermolyses. The TGA results for **3** reveal a ceramic yield of 33.8% at 500 °C that is slightly below the calculated yields for $2MoO_3\cdot B_2O_3\cdot 4SiO_2$ (40.5%) and $2MoO_{1.5}\cdot B_2O_3\cdot 4SiO_2$ (37.3%). Thermogravimetric analysis of **6** reveals a ceramic yield at 600 °C (26.2%) that is significantly lower than that calculated for formation of $2MoO_3\cdot B_2O_3\cdot 4SiO_2\cdot P_2O_5$ (41.0%) or $2MoO_{1.5}\cdot B_2O_3\cdot 4SiO_2\cdot P_2O_5$ (38.3%), suggesting a complex decomposition process and loss of $HOSi(O^tBu)_3$. Despite these complicated results on the thermolyses of **3** and **6**, these species may be useful as sources of isolated Mo/B/Si/O or Mo/B/P/Si/O sites via grafting reactions with oxide supports.[28,29]

Thermolysis of a toluene-d_8 solution of **4a** (in a sealed NMR tube with Cp_2Fe as a standard) at 140 °C led to clean elimination of 7.2 equiv of CH_2CMe_2 (8 are expected) and the formation of an insoluble oxide material. It is noteworthy that $HNMe_2$ (from hydrolysis of Mo−NMe_2 linkages) is not observed in solution upon thermal decomposition of **4a**, suggesting that it may be adsorbed onto the surface of the resultant material due to strong N−Mo interactions (see below). The TGA trace of **4a** (under N_2 at 10 °C min^{-1}) exhibits a precipitous weight loss beginning at 150 °C, corresponding to a ceramic yield of 54.3% at 200 °C (Figure 8). This yield is close to that expected for $2MoO_{1.5}\cdot 2P_2O_5\cdot 2HNMe_2$

(27) Dazhuang, L.; Lixiong, Z.; Biguang, Y.; Jiaofeng, L. *Appl. Catal. A* **1993**, *105*, 185.
(28) (a) Coles, M. P.; Lugmair, C. G.; Terry, K. W.; Tilley, T. D. *Chem. Mater.* **2000**, *12*, 122. (b) Jarupatrakorn, J.; Tilley, T. D. *J. Am. Chem. Soc.* **2002**, *124*, 8380.
(29) (a) Morey, M. S.; Bryan, J. D.; Schwarz, S.; Stucky, G. D. *Chem. Mater.* **2000**, *12*, 3435. (b) Johnson, B. J. S.; Stein, A. *Inorg. Chem.* **2001**, *40*, 801.

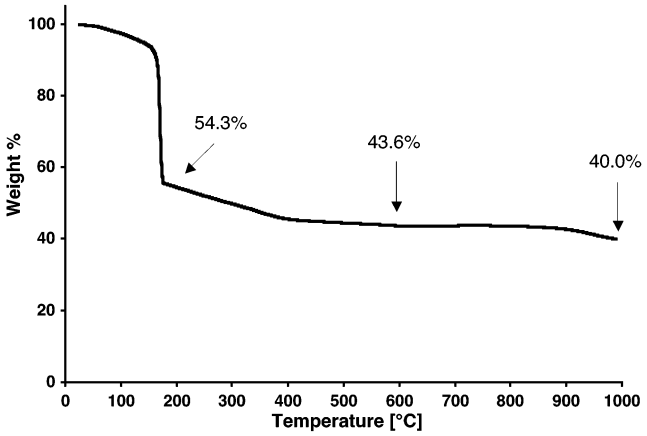

Figure 8. TGA trace of **4a** under N_2 with a heating rate of 10 °C min^{-1}.

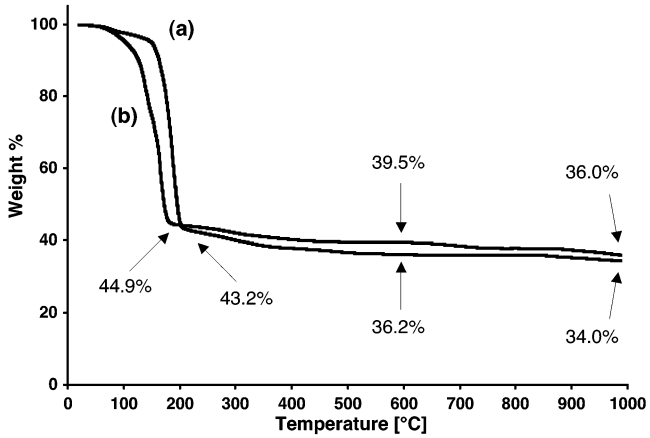

Figure 9. TGA traces of (a) **5a** and (b) **5b** under N_2 with heating rates of 10 °C min^{-1}.

(55.0%). For further comparison, the ceramic yield for formation of $2MoO_3 \cdot 2P_2O_5 \cdot 2HNMe_2$ is 59.3%. A second region of weight loss (10.8%) from 200 to 600 °C is presumably due to removal of adsorbed $HNMe_2$. The ceramic yield at 500 °C (43.6%) is closer to that calculated for $2MoO_{1.5} \cdot 2P_2O_5$ (46.9%) than it is to the calculated yield for $2MoO_3 \cdot 2P_2O_5$ (51.2%), suggesting that Mo may exist in a reduced state. A weight loss of 3.6% is observed from 600 to 1000 °C, indicative of only minor loss of MoO_3 via sublimation (loss of all Mo as MoO_3 would correspond to a 24% weight loss). It is apparent that **4a** is appropriate for use as a single-source molecular precursor to Mo/P/O materials given its clean thermal conversion via the elimination of CH_2CMe_2. The TGA trace of **4b** is similar to that of **4a**, in that there are three regions of weight loss (isobutylene, amine, and MoO_3) at approximately the same temperatures. The ceramic yield of 52.1% at 200 °C is close to that expected for formation of $2MoO_{1.5} \cdot 2P_2O_5 \cdot 2HNMe_2$ (55.0%), and the yield at 600 °C (43.0%) is near the value calculated for $2MoO_{1.5} \cdot 2P_2O_5$ (46.9%). The mass loss between 600 and 1000 °C for **4b** (7.7%) is larger than that observed for **4a**, but still much less than that expected if all of the Mo had been lost as MoO_3 (24.2%).

Thermolysis of a toluene-d_8 solution of **5a** (in a sealed NMR tube with Cp_2Fe as a standard) at 130 °C resulted in the evolution of large amounts of CH_2CMe_2 (5.1 equiv) and the formation of an insoluble precipitate. Significant amounts of $HOSi(O^tBu)_3$ and ^{t}BuOH (0.6 and 0.9 equiv, respectively) were initially observed, presumably resulting from hydrolytic processes. Subsequent heating led to thermal decomposition of the $HOSi(O^tBu)_3$ and the formation of additional CH_2CMe_2, suggesting that Si is incorporated into the growing inorganic network.

Similar results were obtained for the thermolysis of **5b** in toluene-d_8, which resulted in evolution of 4.4 equiv of CH_2CMe_2, 0.5 equiv of $HOSi(O^tBu)_3$, and 0.1 equiv of ^{t}BuOH after heating at 130 °C for 4 h. After heating at 150 °C for an additional 68 h, 7.9 equiv of CH_2CMe_2 and 0.5 equiv of ^{t}BuOH were the only products formed, indicating that the thermal conversion results in incorporation of all the Mo, P, and Si into the final material. No $HNMe_2$ was observed in the ^{1}H NMR spectra taken during the course of the thermolyses.

The TGA traces for **5a** and **5b** exhibit precipitous mass losses at 168 and 142 °C, respectively (Figure 9). The ceramic yields for **5a** and **5b** (at 600 °C) are 36.2 and 39.5%, respectively. For comparison, the calculated ceramic yields for $2MoO_3 \cdot P_2O_5 \cdot 2SiO_2$ and $2MoO_{1.5} \cdot P_2O_5 \cdot 2SiO_2$ are 44.9 and 41.0%, respectively. Thus, the experimental ceramic yields are slightly lower than the calculated values, presumably due to loss of $HOSi(O^tBu)_3$. The gradual loss in mass from ~200 to 600 °C (**5a**, 7.0%; **5b**, 5.4%) is near that expected for removal of 2 equiv of $HNMe_2$ (7.4%). The loss of MoO_3 is very low for both **5a** (2.2%) and **5b** (3.5%). Although the TGA results suggest that solid-state thermolyses of **5a** and **5b** would not lead to total incorporation of all Si (due to small losses of $HOSi(O^tBu)_3$), the complete thermal transformations of **5a** and **5b** in solution are expected to cleanly provide Mo/P/Si/O materials.

Xerogel Formations from 4a, 5a, and 5b. Significant quantities of new materials were obtained by solution (toluene) thermolyses of **4a**, **5a**, and **5b**. A typical preparation involved heating a toluene solution of the molecular precursor, sealed in a thick-walled pyrolysis tube, at 150 °C for ~90 h. In all cases, a monolithic gel formed. The gels were transferred to Schlenk tubes and dried under flowing N_2 for 72 h and then in vacuo for 24 h at 120 °C. This procedure gave uncalcined xerogels $\mathbf{MoOP_{xg}}$ (from **4a**), ***t*-MoOPOSi$_{xg}$** (from **5a**), and ***c*-MoOPOSi$_{xg}$** (from **5b**). All of these uncalcined xerogels react with air/H_2O to give blue Mo oxides. Thus, the xerogels were handled and stored under a moisture-free atmosphere of N_2, unless otherwise noted. The xerogel $\mathbf{MoOP_{xg}}$ is yellow/brown and the $\mathbf{MoOPOSi_{xg}}$ materials are black. In general, the properties of ***t*-MoOPOSi$_{xg}$** and ***c*-MoOPOSi$_{xg}$** are quite similar (Table 1).

Elemental analysis of the uncalcined xerogel derived from **4a** ($\mathbf{MoOP_{xg}}$) reveals C, H, and N contents that correspond to the expected amount of $HNMe_2$, assuming that all of the $HNMe_2$ is retained in the material (Table 1). The uncalcined xerogels derived from **5a** and **5b** have C, H, and N contents that also suggest the presence of 2 equiv of $HNMe_2$ per formula unit. However, the carbon content of these samples is higher than expected, possibly due to the presence of residual organic components (e.g., $-O^tBu$ groups) and/or limited carbide formation. Elemental analyses of $\mathbf{MoOP_{xg}}$ also reveal that the Mo/P ratio is 1:2.04, indicating complete incorporation of Mo and P from the single-source molecular precursor. Similar results were obtained from analysis

Table 1. Properties of the Xerogels Derived from 4a, 5a, and 5b

	combustion analysis (%)[a]			TGA (% loss)[b]		surface area ($m^2\ g^{-1}$)[c]			pore volume ($cm^3\ g^{-1}$)[c]		
sample	C	H	N	<600 °C	>800 °C	unc	300 °C	500 °C	unc	300 °C	500 °C
$MoOP_{xg}$											
estimated	7.8	2.3	4.6	14.7	43.5						
observed	7.3	2.1	4.2	16.4	4.8	165	40	35	0.33	0.13	0.12
***t*-$MoOPOSi_{xg}$**											
estimated	8.1	2.4	4.7	15.2	45.0						
observed	12.7	2.4	3.5	17.3	11.0	260	<5	<5	0.19	0	0
***c*-$MoOPOSi_{xg}$**											
estimated	8.1	2.4	4.7	15.2	45.0						
observed	11.4	2.8	3.3	17.4	8.0	270	<5	<5	0.20	0	0

[a] Estimations are for 2 $HNMe_2$ with 1.5 O per Mo. Analyses are of as-synthesized (dried) samples. [b] Estimated values are for loss of 2 $HNMe_2$ (<600 °C) or all Mo as MoO_3 (>800 °C). [c] Samples are as-synthesized and dried (unc), and calcined at 300 or 500 °C under O_2 for 2 h.

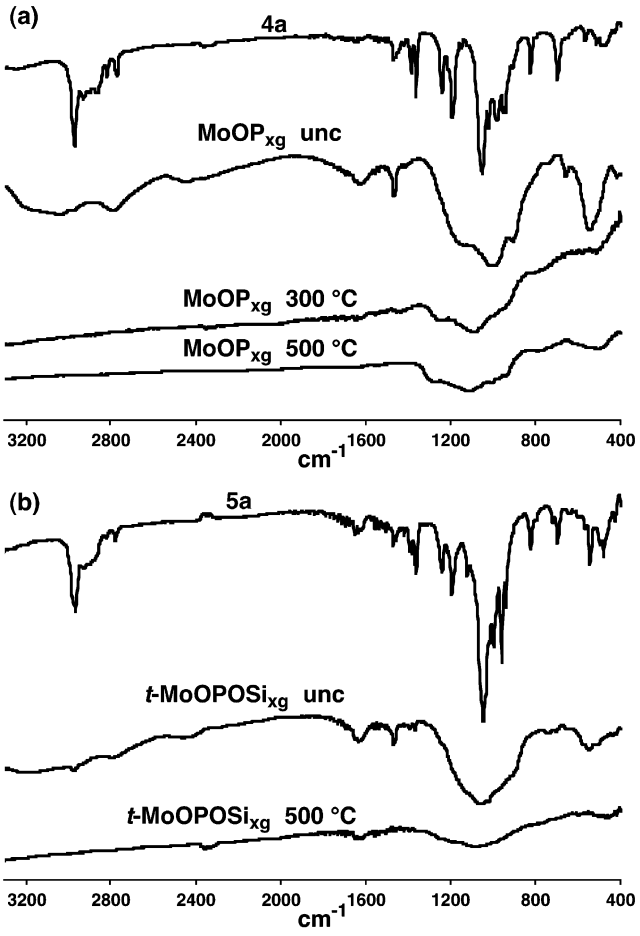

Figure 10. IR spectra of (a) **4a** and **$MoOP_{xg}$** and (b) **5a** and ***t*-$MoOPOSi_{xg}$**.

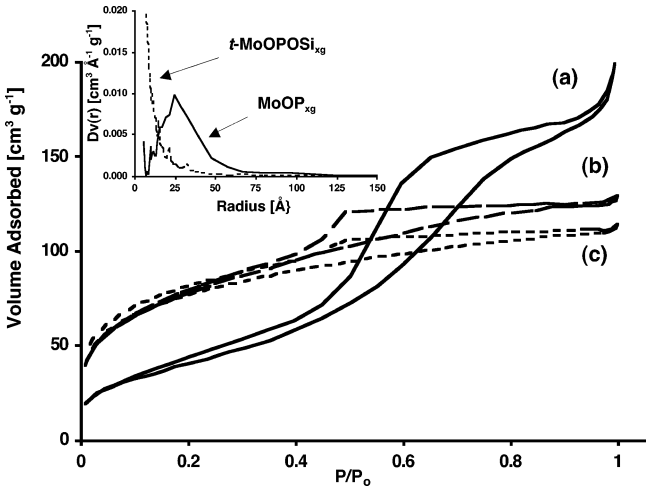

Figure 11. N_2 porosimetry adsorption−desorption isotherms for (a) **$MoOP_{xg}$**, (b) ***c*-$MoOPOSi_{xg}$**, and (c) ***t*-$MoOPOSi_{xg}$**, and BJH pore size distributions for **$MoOP_{xg}$** and ***t*-$MoOPOSi_{xg}$** (inset).

of ***t*-$MoOPOSi_{xg}$**, which revealed a Mo/P/Si ratio of 1:1.03:1.03.

Infrared spectra of **$MoOP_{xg}$** and ***t*-$MoOPOSi_{xg}$** contain broad bands corresponding to $HNMe_2$ (~2800 cm^{-1} and ~3150 cm^{-1}), ^{t}BuO groups (~2900 cm^{-1}), and various E−O, E−O−E, E−O−Mo, and Mo−O linkages (400−1400 cm^{-1}), as shown in Figure 10. Calcination of the xerogels under O_2 led to loss of the IR bands attributed to $HNMe_2$ and the organic components. Bands for Mo−O−Mo species are typically observed at ~880 cm^{-1}, those for Mo−oxo species are found from ~950 to 1000 cm^{-1}, and a characteristic band for bulk MoO_3 has been reported at 820 cm^{-1}.[30] The absence of bands at ca. 820 cm^{-1} in the IR spectra of **$MoOP_{xg}$** and ***t*-$MoOPOSi_{xg}$** suggests that little or no MoO_3 is present in these samples.[30]

Thermogravimetric analyses (10 °C min^{-1} under O_2) of **$MoOP_{xg}$**, ***t*-$MoOPOSi_{xg}$**, and ***c*-$MoOPOSi_{xg}$** reveal weight losses that correspond closely to the expected amounts of C, H, and N (from loss of coordinated $HNMe_2$; Table 1). Interestingly, these TGA results show that only small amounts of MoO_3 are lost from the xerogels at temperatures above 800 °C, with larger amounts of MoO_3 being lost from ***t*-$MOPOSi_{xg}$** and ***c*-$MOPOSi_{xg}$** (Table 1). For comparison, Mo/Si/O materials tend to lose significant amounts of MoO_3 under these conditions.[6,27] It is noteworthy that the TGA results for **5a** and **5b** revealed that the materials derived from their solid-state decompositions lose less MoO_3 than do the corresponding xerogels derived therefrom (Figure 9).

Nitrogen porosimetry was used to investigate the surface areas and pore volumes of **$MoOP_{xg}$**, ***t*-$MoOPOSi_{xg}$**, and ***c*-$MoOPOSi_{xg}$**. Figure 11 shows the adsorption−desorption isotherms for **$MoOP_{xg}$**, ***c*-$MoOPOSi_{xg}$**, and ***t*-$MoOPOSi_{xg}$**, and Table 1 provides the BET[31] surface areas and pore volumes. The BJH method[32] was used to calculate the pore size distributions using the

(30) (a) Mizuno, N.; Katamura, K.; Yoneda, Y.; Misono, M. *J. Catal.* **1983**, *83*, 384. (b) Li, C.; Xin, Q.; Wang, K.-L.; Guo, X. *Appl. Spectrosc.* **1991**, *45*, 874. (c) Dong, W.; Dunn, B. *J. Mater. Chem.* **1998**, *8*, 665.

(31) Brunauer, S.; Emmett, P. H.; Teller, E. *J. Am. Chem. Soc.* **1938**, *60*, 309.

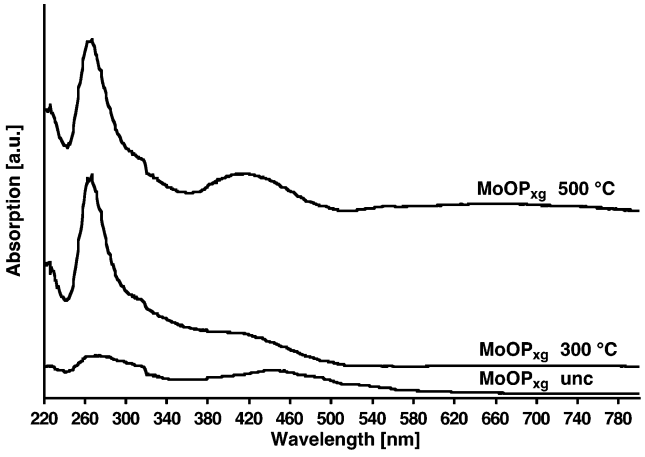

Figure 12. DRUV−vis spectra of **MoOP$_{xg}$**.

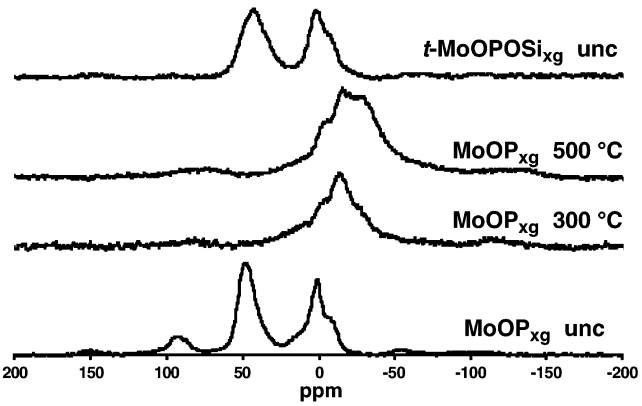

Figure 13. ^{31}P MAS NMR spectra of **MoOP$_{xg}$** and ***t*-MoOPOSi$_{xg}$**.

adsorption branch of the adsorption−desorption isotherm as shown in Figure 11 (inset) for **MoOP$_{xg}$** and ***t*-MoOPOSi$_{xg}$**. These analyses indicate that **MoOP$_{xg}$** contains significant mesoporosity with an average pore radius of 25 Å, whereas ***t*-MoOPOSi$_{xg}$** and ***c*-MoOPOSi$_{xg}$** are primarily microporous with average pore radii <5 Å. The surface areas of the uncalcined xerogels are quite high; however, the pore volumes are somewhat low (Table 1). Calcination of **MoOP$_{xg}$** at 300 °C results in loss of significant surface area (to 40 $m^2\ g^{-1}$) and subsequent calcination at 500 °C reduces the area only slightly to 35 $m^2\ g^{-1}$. An even more dramatic decrease in surface area is observed for ***t*-MoOPOSi$_{xg}$** and ***c*-MoOPOSi$_{xg}$** upon calcination at 300 or 500 °C (Table 1). Despite this decrease in surface area, powder X-ray diffraction studies of **MoOP$_{xg}$**, ***t*-MoOPOSi$_{xg}$**, and ***c*-MoOPOSi$_{xg}$** reveal that these materials are amorphous, even after calcination at 500 °C.

Diffuse-reflectance UV−vis (DRUV−vis) spectroscopy was performed on **MoOP$_{xg}$**, ***t*-MoOPOSi$_{xg}$**, and ***c*-MoOPOSi$_{xg}$** to investigate the nature of the Mo species. It is recognized that the local Mo^{6+} coordination environment in supported molybdenum species has little influence over the position of bands in DRUV−vis spectra.[33] However, the degree of dispersion of the Mo species (size of MoO_x species and the distance between them) does influence the DRUV−vis band positions, with higher wavelength absorptions observed for larger polymolybdate aggregates and MoO_3.[33] Bands from 200 to 400 nm are characteristic of O^{2-} to Mo^{6+} charge-transfers.[33] Figure 12 shows the DRUV−vis spectra of **MoOP$_{xg}$** in its uncalcined state and after calcination at 300 and 500 °C under O_2. Very weak (and broad) absorption bands are observed at 275 and 450 nm for uncalcined **MoOP$_{xg}$**, suggesting that few Mo^{6+} species are present. After calcination at 300 °C, a strong (and sharp) band at 265 nm and a broad band at 425 nm are evident, and a strong (and sharp) band at 265 nm and a strong (and broad) band at 415 nm are present after calcination at 500 °C, indicating formation of increasing amounts of Mo^{6+} species with increasing calcination temperature. Also, the gradual shift of all absorption bands to higher energy with increasing calcination temperature suggests formation of Mo sites that are more isolated,[33] presumably resulting from separation of Mo_2 species (via formation of Mo−O−Mo linkages and isolated MoO_x species) that are initially in close contact due to their dimolybdenum molecular precursor origin. Unfortunately, the intense black coloration of ***t*-MoOPOSi$_{xg}$** and ***c*-MoOPOSi$_{xg}$** prevented the acquisition of meaningful DRUV−vis spectra for these materials.

Solid-state magic angle spinning (MAS) ^{31}P NMR studies of **MoOP$_{xg}$** and ***t*-MoOPOSi$_{xg}$** reveal that the as-synthesized (dried) materials contain broad peaks in two main regions (Figure 13). Interestingly, these primary resonances (at ca. 45 and 0 ppm) correspond closely to the chemical shifts exhibited (in solution) for the bridging (ca. 25 ppm) and terminal (ca. −5 ppm) $-O_2P(O^tBu)_2$ ligands in **4a**, **4b**, **5a**, **5b**, and **6**. This suggests the presence of bridging and terminal phosphate groups in the ceramic material after mild thermal treatments, and that structural features of the molecular precursor are transferred to the material formed therefrom. Further, the presence of ^{31}P MAS NMR resonances corresponding to bridging phosphate ligands suggests that the Mo−Mo interaction of the molecular precursors remain intact upon conversion to the materials. The bridging and terminal resonances in the ^{31}P MAS NMR spectrum of ***t*-MoOPOSi$_{xg}$** (derived from **5a**, having only bridging phosphate groups) suggest that, under the thermolytic conditions, cleavage of the phosphate bridges (to form terminal phosphates) is significant (∼50:50 ratio of the two species). After calcination at 300 °C under O_2, the ^{31}P environments closely resemble those typical for inorganic phosphate materials, with broad resonances from −50 to 20 ppm.[34]

Catalytic Oxidative Dehydrogenation of Propane. Molybdenum-containing oxide materials (i.e., MoO_x species supported on Al_2O_3, ZrO_2, SiO_2, SiO_2/TiO_2, NiO, Sb_2O_3, Bi_2O_3, and MgO, etc.) have been previously examined as catalysts for the oxidative dehydrogenation of propane to propylene.[35] Although vanadium-based oxide materials appear to be the most efficient catalysts known for the oxidative dehydrogenation of propane,[36] many of the molybdenum-based systems have shown promise with respect to their selectivities. These results,

(32) Barret, E. P.; Joyner, L. G.; Halenda, P. P. *J. Am. Chem. Soc.* **1951**, *73*, 3, 373.

(33) (a) Fournier, M.; Louis, C.; Che, M.; Chaquin, P.; Masure, D. *J. Catal.* **1989**, *119*, 400. (b) Louis, C.; Che, M. *J. Phys. Chem.* **1987**, *91*, 2875. (c) Williams, C. C.; Ekerdt, J. G. *J. Phys. Chem.* **1991**, *95*, 8781. (d) Williams, C. C.; Ekerdt, J. G. *J. Phys. Chem.* **1991**, *95*, 8791. (e) Bañares, M. A.; Hu, H.; Wachs, I. E. *J. Catal.* **1994**, *150*, 407.

(34) Iwamoto, R.; Fernandez, C.; Amoureux, J. P.; Grimblot, J. *J. Phys. Chem. B* **1998**, *102*, 4342.

Table 2. Properties of the Xerogels Derived from Cothermolyses of 4a and Bi[OSi(O^{t}Bu)$_3$]$_3$

	combustion analysis (%)[a]			TGA (% loss)[b]		surface area (m^2 g^{-1})[c]			pore volume (cm^3 g^{-1})[c]		
sample	C	H	N	<600 °C	>800 °C	unc	300 °C	500 °C	unc	300 °C	500 °C
BiMoPSi$_{2:1}$											
estimated	3.4	1.0	2.0	6.4	17.8						
observed	4.4	0.04	0.45	8.4	10.6	380	280	35	0.76	0.59	0.12
BiMoPSi$_{4:1}$											
estimated	2.3	0.70	1.3	4.3	11.0						
observed	8.7	0.20	0.81	14.0	8.5	500	360	50	0.53	0.36	0.07
BiMoPSi$_{8:1}$											
estimated	1.3	0.35	0.72	2.4	6.3						
observed	10.6	1.0	0.45	14.2	2.4	480	355	60	0.42	0.28	0.08

[a] Estimations are for 2 $HNMe_2$ with 1.5 O per Mo. Analyses are of as-synthesized (dried) samples. [b] Estimated values are for loss of 2 $HNMe_2$ (<600 °C) or all Mo as MoO_3 (>800 °C). Adsorbed H_2O (upon transfer to the instrument) and carbon deposits may be responsible for the higher than expected losses at temperatures <600 °C. [c] Samples are as-synthesized and dried (unc), and calcined at 300 or 500 °C under O_2 for 2 h.

coupled with the well-known selective oxidation properties of molybdenum-containing oxide materials in other catalytic reactions,[2c,d,e,17,19] prompted us to study **MoOP$_{xg}$** as a heterogeneous catalyst under propane ODH conditions.

The catalytic efficiency of **MoOP$_{xg}$**, after calcination at 500 °C under O_2 or He, for the oxidative dehydrogenation of propane was examined at 450 °C. The reactions were run at low propane conversion in order to determine the intrinsic activities (at infinite flow rate) and intrinsic selectivities (at 0% conversion) for propylene formation.[37] The intrinsic activities (3.2 and 3.7 mmol propylene produced g^{-1} h^{-1} for **MoOP$_{xg}$** calcined under O_2 and He, respectively) and selectivities (35.8 and 28.2% for **MoOP$_{xg}$** calcined under O_2 and He, respectively) are low, regardless of calcination conditions. The low activity presumably results from the low surface area of the catalyst (35 m^2 g^{-1}), and the poor selectivity is likely a result of propylene combustion processes.

Several molybdenum-containing partial oxidation catalysts also have bismuth as a component.[2c,d,e,35r] With this in mind, cothermolyses of **4a** and the previously reported bismuth siloxide Bi[OSi(O^{t}Bu)$_3$]$_3$[5d] were performed in solution (toluene) to generate xerogels with the approximate compositions $Bi_2Mo_2P_4Si_6O_{28}$ (**BiMoPSi$_{2:1}$**), $Bi_4Mo_2P_4Si_{12}O_{43}$ (**BiMoPSi$_{4:1}$**), and $Bi_8Mo_2P_4Si_{24}O_{73}$ (**BiMoPSi$_{8:1}$**). The as-synthesized (and dried) Bi/Mo/P/Si/O xerogels are all dark brown; however, calcination at 300 °C under O_2 results in the formation of green (**BiMoPSi$_{2:1}$**), yellow-green (**BiMoPSi$_{4:1}$**), and yellow (**BiMoPSi$_{8:1}$**) materials. Further calcination at 500 °C does not alter these colors. All of these xerogels have high surface areas in their as-synthesized state (from 380 to 500 m^2 g^{-1}), however calcination yields materials with significantly reduced surface areas (from 35 to 60 m^2 g^{-1} at 500 °C). Table 2 provides a summary of the properties of the Bi/Mo/P/Si/O xerogels. Combustion analyses of the as-synthesized xerogels suggest that most of the $HNMe_2$ evolved upon conversion of the precursors to materials is not retained, contrary to what is observed upon formation of **MoOP$_{xg}$**. For example, the nitrogen contents of **BiMoPSi$_{2:1}$**, **BiMoPSi$_{4:1}$**, and **BiMoPSi$_{8:1}$** in their as-synthesized (and dried) states are 0.45, 0.81, and 0.45%, respectively. The nitrogen contents calculated for materials containing 1 equiv of $HNMe_2$ per molybdenum atom are 2.0% for **BiMoPSi$_{2:1}$**, 1.3% for **BiMoPSi$_{4:1}$**, and 0.72% for **BiMoPSi$_{8:1}$**. The carbon contents for these samples are relatively high, but calcination at 300 °C is sufficient to remove all of the organic species. Infrared spectra of as-synthesized (and dried) **BiMoPSi$_{2:1}$**, **BiMoPSi$_{4:1}$**, and **BiMoPSi$_{8:1}$** confirm the presence of organic components, presumably in the form of small amounts of $HNMe_2$ and residual $-O^tBu$ groups.

Propane ODH reactions were investigated with Bi/Mo/P/Si/O materials that were calcined under O_2 at 500 °C. These studies reveal that **BiMoPSi$_{2:1}$** and **BiMoPSi$_{4:1}$** are active as ODH catalysts at 450 °C, whereas **BiMoPSi$_{8:1}$** exhibits no appreciable activity (Table 3). On a per gram basis, catalyst activity decreases with decreasing molybdenum content for **MoOP$_{xg}$**, **BiMoPSi$_{2:1}$**, and **BiMoPSi$_{4:1}$**. Intrinsic selectivities for propylene formation at 450 °C using **BiMoPSi$_{2:1}$** (77.2%) and **BiMoPSi$_{4:1}$** (79.0%) are significantly higher than that for **MoOP$_{xg}$** (35.8%). Performing the ODH reaction at 500 °C using the Bi/Mo/P/Si/O catalysts reveals increased activities for **BiMoPSi$_{2:1}$** and **BiMoPSi$_{4:1}$**, with **BiMoPSi$_{8:1}$** still being inactive (Table 3). Hence, when compared to **MoOP$_{xg}$**, the addition of bismuth to the catalyst adds significant improvements to the selectivity for propylene formation; however, the activity remains low. Addition of large amounts of bismuth appears to have detrimental effects in terms of catalyst activity, with **BiMoPSi$_{8:1}$** having no measurable ODH activity under the conditions employed.

(35) (a) Chen, K.; Bell, A. T.; Iglesia, E. *J. Catal.* **2002**, *209*, 35. (b) Chen, K.; Iglesia, E.; Bell, A. T. *Stud. Surf. Sci. Catal.* **2001**, *136*, 507. (c) Watson, R. B.; Ozkan, U. S. *Stud. Surf. Sci. Catal.* **2001**, *136*, 221. (d) Chen, K.; Xie, S.; Bell, A. T.; Iglesia, E. *J. Catal.* **2001**, *198*, 232. (e) Abello, M. C.; Gomez, M. F.; Ferretti, O. *Appl. Catal. A* **2001**, *207*, 421. (f) Chen, K.; Iglesia, E.; Bell, A. T. *J. Phys. Chem. B* **2001**, *105*, 646. (g) Cadus, L.; Ferretti, O. *Catal. Lett.* **2000**, *69*, 199. (h) Chen, K.; Xie, S.; Bell, A. T.; Iglesia, E. *J. Catal.* **2000**, *195*, 244. (i) Watson, R. B.; Ozkan, U. S. *J. Catal.* **2000**, *191*, 12. (j) Chen, K.; Xie, S.; Bell, A. T.; Iglesia, E. *J. Catal.* **2000**, *189*, 421. (k) Miller, J. E.; Jackson, N. B.; Evans, L.; Sault, A. G.; Gonzales, M. M. *Catal. Lett.* **1999**, *58*, 147. (l) Gomez, M. F.; Cadus, L. E. *Catal. Lett.* **1998**, *53*, 185. (m) Meunier, F. C.; Yasmeen, A.; Ross, J. R. H. *Catal. Today* **1997**, *37*, 33. (n) Stern, D. L.; Grasselli, R. K. *J. Catal.* **1997**, *167*, 550. (o) Parmaliana, A.; Sokolovskii, V.; Arena, F.; Frusteri, F.; Miceli, D. *Catal. Lett.* **1996**, *40*, 105. (p) Yoon, Y. S.; Ueda, W.; Moroka, Y. *Catal. Lett.* **1995**, *35*, 57. (q) Grabowski, R.; Grzybowska, B.; Samson, K.; Sloczynski, J.; Stoch, J.; Wcislo, K. *Appl. Catal. A* **1995**, *125*, 129. (r) Barrault, J.; Maguad, L.; Ganne, M.; Tournoux, M. *Stud. Surf. Sci. Catal.* **1994**, *82*, 305.

(36) (a) Rulkens, R.; Tilley, T. D. *J. Am. Chem. Soc.* **1998**, *120*, 9959. (b) Rulkens, R.; Male, J. L.; Terry, K. W.; Olthof, B.; Khodakov, A.; Bell, A. T.; Iglesia, E.; Tilley, T. D. *Chem. Mater.* **1999**, *11*, 2966. (c) Pak, C.; Bell, A. T.; Tilley, T. D. *J. Catal.* **2002**, *206*, 49.

(37) (a) Khodakov, A.; Yang, J.; Su, S.; Iglesia, E.; Bell, A. T. *J. Catal.* **1998**, *177*, 343. (b) Khodakov, A.; Olaf, B.; Bell, A. T.; Iglesia, E. *J. Catal.* **1999**, *181*, 205.

Table 3. Propane ODH Results Utilizing the Catalysts Derived from 4a and Bi[OSi(O^{t}Bu)$_3$]$_3$

	intrinsic activity (mmol g^{-1} h^{-1})[a]		intrinsic selectivity (%)[b]		activity (mmol g^{-1} h^{-1})[d]		selectivity (%)[d]	
catalyst	450 °C	500 °C	450 °C	500 °C	450 °C	500 °C	450 °C	500 °C
BiMoPSi$_{2:1}$	2.3	4.9	77.2[c]	63.3	1.3	3.4	70.0	69.6
BiMoPSi$_{4:1}$	0.70	1.0	79.0[c]	54.1	0.45	0.70	63.4	48.3
BiMoPSi$_{8:1}$	0	0	N/A	N/A	0	0	N/A	N/A
MoOP$_{xg}$ O_2	3.2		35.8		1.6		21.5	
MoOP$_{xg}$ He	3.7		28.2		3.2		20.9	

[a] Activity (mmol propylene produced per gram of catalyst per hour) at a reaction temperature of 450 or 500 °C (Bi-containing) or after calcination under O_2 or He (**MoOP$_{xg}$**). [b] Selectivity (% propylene) at a reaction temperature of 450 or 500 °C (Bi-containing) or after calcination under O_2 or He (**MoOP$_{xg}$**). [c] Selectivity at 0% propane conversion not including data at very low propane conversions (where the selectivity is 100%). [d] Activity or selectivity observed at ~0.2% (450 °C) or ~0.6% (500 °C) propane conversion.

Concluding Remarks

The syntheses and structural characterizations of several new triply bonded dimolybdenum(III) complexes containing the −OSi(O^{t}Bu)$_3$, −O$_2$P(O^{t}Bu)$_2$, and −OB[OSi(O^{t}Bu)$_3$]$_2$ ligands were achieved. Of note are the structural characterizations of two geometric isomers for both **4** and **5** that are, to our knowledge, the first such examples for the Mo_2^{6+} fragment. The transfer of −OSi(O^{t}Bu)$_3$ from the −OB[OSi(O^{t}Bu)$_3$]$_2$ ligand to a metal center appears to represent a general reaction path for this ligand, as evidenced by the formation of **2** upon reaction of **3** with 4 equiv of ^{t}BuOH, upon addition of HOB[OSi(O^{t}Bu)$_3$]$_2$ to Mo$_2$(O^{t}Bu)$_6$, and by the previously reported quantitative conversion of Cp$_2$Zr(Me)OB[OSi(O^{t}Bu)$_3$]$_2$ to Cp$_2$Zr[OSi(O^{t}Bu)$_3$]$_2$.[10] It appears that the nature of the additional ligands present on the metal center has great influence over the decomposition pathway of complexes containing the −OB[OSi(O^{t}Bu)$_3$]$_2$ ligand, and we are continuing to investigate the syntheses and chemistry of such species.

Several of the complexes isolated here appear to be well-suited as single-source molecular precursors to materials containing molybdenum with various combinations of other heteroelements. In particular, **2**, **4a**, **5a**, and **5b** appear promising as molecular precursors to Mo/Si/O, Mo/P/O, and Mo/P/Si/O materials, respectively, due to their clean thermal decompositions (by NMR and TGA). To demonstrate this, solution thermolyses of **4a**, **5a**, and **5b** were used to produce xerogels (upon drying) with high surface areas and interesting properties. Complete incorporation of all P, Si (for **5a** and **5b**), and Mo is observed, providing further evidence that the conversions to multicomponent oxides are efficient and clean. The as-synthesized materials in each case appear to retain structural features of their respective starting molecular precursors, as indicated by ^{31}P MAS NMR and DRUV−vis spectroscopies. This observation suggests that the nature of the starting molecular precursor can strongly influence the final structure and properties of the materials derived therefrom. There do not appear to be any obvious differences in the physical properties of the materials synthesized from the trans and cis isomers of **5**.

Although the xerogels **MoOP$_{xg}$**, ***t*-MoOPOSi$_{xg}$**, and ***c*-MoOPOSi$_{xg}$** are not efficient catalysts for the ODH of propane, these materials may have applications as partial oxidation catalysts for moderate- to low-temperature reactions (<300 °C), especially considering their high surface areas after calcination under mild conditions.[17] Cothermolyses of **4a** and Bi[OSi(O^{t}Bu)$_3$]$_3$ give Bi/Mo/P/Si/O xerogels that exhibit improved selectivity for propylene formation in propane ODH. However, larger amounts of Bi appear to be detrimental, resulting in no measurable ODH activity. Further cothermolyses of **2**, **4a**, **5a**, or **5b** with other complexes appropriate for use in the TMP route (i.e., other M[OSi(O^{t}Bu)$_3$]$_n$ and M[O$_2$P(O^{t}Bu)$_2$]$_n$ complexes)[5,6,7,9,10] may provide additional materials with well-defined (and variable) compositions of use in oxidation, epoxidation, and ammoxidation catalysis.[2c,d,e,17,19]

Experimental Section

General. All synthetic manipulations were performed under an atmosphere of nitrogen using standard Schlenk techniques and/or a Vacuum Atmospheres drybox, unless noted otherwise. All solvents used were distilled from sodium/benzophenone, potassium/benzophenone, sodium, or calcium hydride as appropriate. The solution NMR spectra were recorded at ambient temperature on a Bruker AMX300 spectrometer at 300 (^{1}H) or 75.5 (^{13}C) MHz, or on a Bruker AMX400 spectrometer at 400 (^{1}H), 100.6 (^{13}C), or 161.9 (^{31}P) MHz. Chemical shifts are reported in ppm relative to tetramethylsilane (^{1}H and ^{13}C) and H_3PO_4 (^{31}P). Benzene-d_6, vacuum transferred from a Na/K alloy, was used as the solvent for all NMR studies. Infrared spectra were recorded using a Mattson Infinity Series FTIR spectrometer with all samples pressed into KBr disks. Thermal analyses were performed using a TA Instruments SDT 2960 integrated thermogravimetric/differential scanning calorimetric analyzer (TGA/DSC). N_2 porosimetry measurements were performed using a Quantachrome Autosorb-1 surface area analyzer with samples heated at 120 °C, under reduced pressure, for a minimum of 8 h immediately prior to data collection. PXRD data were collected using a Siemens D5000 diffractometer operating with $\theta-2\theta$ geometry at 25 °C (Cu Kα radiation, 1.5 s collection time, and 0.02° step size). DRUV−vis spectra were acquired using a Perkin-Elmer Lambda-9 spectrophotometer, a slit width of 4 nm, and a collection speed of 120 nm min^{-1}. Solid-state ^{31}P magic angle spinning (MAS) NMR spectra were recorded at the University of California, Davis using a Chemagnetics CMX 400 spectrometer operating at a frequency of 161.98 MHz. The samples were loaded into a 4-mm ZrO_2 rotor and spun at the magic angle with a rate of 14.0 kHz, a 4-μs pulse length ($\pi/2$), and a relaxation delay of 30 s. Elemental analyses were performed by the College of Chemistry Micro-Mass Facility at the University of California, Berkeley (C, H, N) or by Galbraith Laboratories, Knoxville, TN (Mo, P, Si). The starting materials HOSi(O^{t}Bu)$_3$,[38] HOP(O)(O^{t}Bu)$_2$,[39] HOB[OSi(O^{t}Bu)$_3$]$_2$,[10] Mo$_2$(O^{t}Bu)$_6$,[12b] Mo$_2$(NMe$_2$)$_6$,[12c] and Bi[OSi(O^{t}Bu)$_3$]$_3$[5d] were prepared by literature procedures.

Mo$_2$(NMe$_2$)$_4$[OSi(O^{t}Bu)$_3$]$_2$ (1). To a stirred pentane (10 mL) solution of Mo$_2$(NMe$_2$)$_6$ (0.537 g, 1.18 mmol) in a Schlenk tube was added (dropwise over 5 min) a pentane (25 mL) solution of HOSi(O^{t}Bu)$_3$ (0.623 g, 2.36 mmol) at 25 °C. The yellow

(38) Abe, Y.; Kijima, I. *Bull. Chem. Soc. Jpn.* **1969**, *42*, 1118.
(39) Goldwhite, H.; Saunders, B. C. *J. Chem. Soc.* **1957**, 2409.

reaction mixture was stirred for an additional 30 min. Subsequent filtration to remove a small amount of a brown/black precipitate, concentration of the filtrate to 15 mL, and cooling to −78 °C led to the formation yellow crystals of **1**. The crystals were isolated, washed with ca. 5 mL of cold (−78 °C) pentane, and dried in vacuo. Three crops of crystals were obtained in a similar manner (with the mother liquor concentrated to ca. 50% volume each time) to give analytically pure **1** in 76% yield (0.804 g, 0.898 mmol). Anal. Calcd for $C_{32}H_{78}Mo_2N_4O_8Si_2$ (%): C, 42.94; H, 8.78; N, 6.26. Found: C, 43.23; H, 9.00; N, 6.09. IR (cm^{-1}): 2973 vs, 2932 m, 2903 m, 2867 m, 2820 w, 2773 w, 1472 w, 1449 w, 1388 m, 1364 s, 1243 s, 1194 s, 1054 vs, 1025 s, 985 s, 954 m, 943 m, 826 m, 699 m, 651 w, 568 w, 515 w, 491 w, 431 w. Two sets of resonances, corresponding to two conformations (a and b), were observed in the solution NMR spectra. ^{1}H NMR (a) δ 4.42 (br, 6 H, NCH_3), 2.75 (br, 6 H, NCH_3), 1.48 (s, 54 H, Si(O^{t}Bu)$_3$); (b) δ 4.17 (s, 6 H, NCH_3), 2.81 (s, 6 H, NCH_3), 1.49 (s, 54 H, Si(O^{t}Bu)$_3$). ^{13}C{^{1}H} NMR (a) δ 71.80 (s, SiO*C*(CH$_3$)$_3$), 31.90 (s, SiOC(*C*H$_3$)$_3$), no N*C*H$_3$ resonances were observed; (b) δ 72.01 (s, SiO*C*(CH$_3$)$_3$), 32.06 (s, SiOC(*C*H$_3$)$_3$), no N*C*H$_3$ resonances were observed.

$Mo_2(O^tBu)_4[OSi(O^tBu)_3]_2$ (2). To a stirred pentane (2 mL) solution of $Mo_2(O^tBu)_6$ (0.069 g, 0.110 mmol) in a Schlenk tube was added (dropwise over 5 min) a pentane (2 mL) solution of $HOSi(O^tBu)_3$ (0.050 g, 0.220 mmol) at 25 °C. The red reaction mixture was stirred for an additional 30 min. Subsequent filtration and cooling to −30 °C led to the formation of **2** as red crystals. The crystals were isolated and washed with ca. 1 mL of cold (−30 °C) pentane and dried in vacuo. Two crops of crystals were obtained to give analytically pure **2** in 59% yield (0.065 g, 0.064 mmol). Anal. Calcd for $C_{40}H_{90}Mo_2O_{12}Si_2$ (%): C, 47.51; H, 8.97. Found: C, 47.56; H, 9.08. IR (cm^{-1}): 2974 vs, 2931 m, 2902 w sh, 2874 w, 1473 w, 1389 m, 1365 s, 1243 s, 1192 s, 1061 vs, 1026 s, 967 s, 950 s, 915 s, 890 m, 829 w, 775 w, 670 m, 658 w, 616 w, 567 w, 513 w, 480 w, 428 w. ^{1}H NMR δ 1.61 (s, 36 H, MoO^{t}Bu), 1.49 (s, 54 H, Si(O^{t}Bu)$_3$). ^{13}C{^{1}H} NMR δ 33.23 (s, MoOC(*C*H$_3$)$_3$), 32.01 (s, SiOC(*C*H$_3$)$_3$). No −O*C*Me$_3$ resonances were observed.

$Mo_2(NMe)_4\{OB[OSi(O^tBu)_3]_2\}_2$ (3). To a stirred pentane (5 mL) solution of $HOB[OSi(O^tBu)_3]_2$ (0.445 g, 0.802 mmol) in a Schlenk tube was added a pentane (5 mL) solution of $Mo_2(NMe_2)_6$ (0.183 g, 0.401 mmol), at 25 °C. The light yellow reaction mixture was filtered, and the filtrate was concentrated to 3 mL and cooled to −30 °C. Yellow crystals of **3** were isolated and washed with ca. 1 mL of cold (−30 °C) pentane and dried in vacuo. Two crops of crystals were obtained to give analytically pure **3** in 73% yield (0.430 g, 0.291 mmol). Anal. Calcd for $C_{56}H_{132}B_2Mo_2N_4O_{18}Si_4$ (%): C, 45.58; H, 9.02; N, 3.80. Found: C, 45.78; H, 9.16; N, 3.92. IR (cm^{-1}): 2975 vs, 2932 m, 2909 m, 2873 m, 2825 w, 2779 w, 1474 w, 1389 m, 1366 s, 1338 m, 1285 w, 1244 m, 1193 s, 1062 vs, 1026 s, 957 w, 945 w, 911 w, 829 m, 701 m, 624 w, 575 w, 516 w, 485 w, 431 w. ^{1}H NMR δ 4.50 (br s, 6 H, NCH_3), 2.87 (br s, 6 H, NCH_3), 1.53 (s, 54 H, Si(O^{t}Bu)$_3$). ^{13}C{^{1}H} NMR δ 72.77 (s, Si(O*C*(CH$_3$)$_3$), 31.93 (s, Si(OC(*C*H$_3$)$_3$). No N*C*H$_3$ resonances were observed.

$Mo_2(NMe_2)_2[\mu\text{-}O_2P(O^tBu)_2]_2[O_2P(O^tBu)_2]_2$ (4a and 4b). To a stirred pentane (5 mL) solution of $HOP(O)(O^tBu)_2$ (0.570 g, 2.71 mmol) in a Schlenk tube was rapidly added a pentane (10 mL) solution of $Mo_2(NMe_2)_6$ (0.309 g, 0.678 mmol) at 25 °C. An orange microcrystalline powder (***trans*-4** (**4a**)) began to precipitate out of solution after ca. 30 s. The reaction mixture was stirred for an additional 10 min, filtered, and the precipitate (**4a**) was washed with 15 mL of pentane. In this isolated microcrystalline form, **4a** was analytically and spectroscopically pure (0.536 g, 0.480 mmol). The mother liquor was cooled to −78 °C and resulted in the isolation of additional **4a** in pure form as orange well-formed crystals (0.022 g, 0.020 mmol) giving a total isolated yield of ***trans*-4** (**4a**) of 74%. Quantitative recrystallization of **4a** was achieved from a pentane solution that was cooled to −78 °C. Cooling the mother liquor to −30 °C for several weeks after isolation of **4a** resulted in the formation of ***cis*-4** (**4b**) as yellow crystals in low yield (<5%). Reaction of $Mo_2(NMe_2)_6$ and 4 equiv of $HOP(O)(O^tBu)_2$ monitored by ^{1}H NMR spectroscopy revealed that only **4a** is formed at 25 °C.

4a. Anal. Calcd for $C_{36}H_{84}Mo_2N_2O_{16}P_4$ (%): C, 38.72; H, 7.58; N, 2.51. Found: C, 38.61; H, 7.63; N, 2.59. IR (cm^{-1}): 2977 vs, 2932 m, ca. 2900 sh w, ca. 2875 sh w, 2829 w, 2785 w, 1476 w, 1459 w, 1393 m, 1368 s, 1252 s, 1216 s, 1183 s, 1098 m, 1056 vs, 1038 vs, 1002 vs, 930 m, 919 m, 830 w, 814 w, 707 m, 595 m, 534 m, 491 w, 438 w. ^{1}H NMR δ 5.32 (s, 6 H, NCH_3), 3.05 (s, 6 H, NCH_3), 1.65 (s, 36 H, *t*-O$_2$P(O^{t}Bu)$_2$), 1.50 (s, 36 H, μ-O$_2$P(O^{t}Bu)$_2$). ^{13}C{^{1}H} NMR δ 77.66 (d, *t*-O$_2$P[O*C*(CH$_3$)$_3$]$_2$, J = 12.5 Hz), 54.71 (s, N(*C*H$_3$)$_2$), 47.01 (s, N(*C*H$_3$)$_2$), 30.58 (d, O$_2$P[OC(*C*H$_3$)$_3$]$_2$, J = 4.3 Hz), 30.29 (m, O$_2$P[OC(*C*H$_3$)$_3$)]$_2$. The μ-PO*C*(CH$_3$)$_3$ resonance was not observed. ^{31}P{^{1}H} NMR δ 22.43 (s, 2 P, μ-O$_2$P(O^{t}Bu)$_2$), −6.90 (s, 2 P, *t*-O$_2$P(O^{t}Bu)$_2$).

4b. IR (cm^{-1}): 2978 vs, 2933 m, ca. 2900 sh w, ca. 2879 sh w, 2789 w, 2724 w, 1474 w, 1458 w, 1395 m, 1369 s, 1252 s, 1182 s, 1046 br vs, 1000 br vs, 917 m, 830 m, 814 w, 720 m, 709 m, 603 w, 549 s, 514 w, 503 w, 478 w. ^{1}H NMR δ 5.05 (s, 6 H, NCH_3), 3.27 (s, 6 H, NCH_3), 1.71 (s, 18 H, t−O$_2$P(O^{t}Bu)$_2$), 1.66 (s, 18 H, *t*-O$_2$P(O^{t}Bu)$_2$), 1.47 (s, 18 H, μ-O$_2$P(O^{t}Bu)$_2$), 1.46 (s, 18 H, μ-O$_2$P(O^{t}Bu)$_2$). ^{31}P{^{1}H} NMR δ 24.42 (s, 2 P, μ-O$_2$P(O-^{t}Bu)$_2$), −6.14 (s, 2 P, *t*-O$_2$P(O^{t}Bu)$_2$).

$Mo_2(NMe_2)_2[OSi(O^tBu)_3]_2[\mu\text{-}O_2P(O^tBu)_2]_2$ (5a and 5b). To a stirred pentane (10 mL) solution of **1** (0.566 g, 0.632 mmol) in a Schlenk tube was added (dropwise over 10 min) a pentane (10 mL) solution of $HOP(O)(O^tBu)_2$ (0.266 g, 1.26 mmol) at 25 °C. The red reaction mixture was stirred for an additional 45 min and subsequently cooled to −78 °C. Analytically and spectroscopically pure red crystals of the less soluble trans isomer of **5** (**5a**) were obtained (washed with 1 mL of pentane) in 38% yield (0.295 g, 0.241 mmol). Concentration of the yellow mother liquor to 3 mL and subsequent cooling to −78 °C led to the isolation of the cis isomer of **5** (**5b**) as yellow crystals containing C_5H_{12} solvate molecules. Placing the crystals under reduced pressure for a brief time resulted in removal of the C_5H_{12} providing spectroscopically and analytically pure **5b** in 23% yield (0.180 g, 0.147). Hence the total yield of **5** (**5a** + **5b**) was 61%. Repeating the reaction five times resulted in the isolation of both **5a** and **5b** in similar yields (±5%) each time.

5a. Anal. Calcd for $C_{44}H_{102}N_2Mo_2N_2O_{16}P_2Si_2$ (%): C, 43.13; H, 8.39; N, 2.29. Found: C, 43.33; H, 8.54; N, 2.40. IR (cm^{-1}): 2969 s, 2931 m, 2903 br w, 2825 w, 2782 w, 1473 w, 1457 w, 1386 w, 1362 m, 1243 m, 1196 s, 1123 m, 1049 vs, 1020 sh s, 1000 s, 961 s, 941 m, 825 m, 723 w, 699 m, 646 w, 545 m, 501 w, 481 m, 428 w. ^{1}H NMR δ 5.61 (s, 6 H, NCH_3), 2.93 (s, 6 H, NCH_3), 1.59 (s, 54 H, Si(O^{t}Bu)$_3$), 1.45 (s, 36 H, μ-O$_2$P(O^{t}Bu)$_2$). ^{13}C{^{1}H} NMR δ 71.39 (s, SiO*C*(CH$_3$)$_3$), 32.03 (s, SiOC(*C*H$_3$)$_3$), 30.31 (d, μ-O$_2$P(OC(*C*H$_3$)$_3$, J = 2.4 Hz). No N*C*H$_3$ or μ-O$_2$P-[O*C*(CH$_3$)$_2$]$_2$ resonances were observed. ^{31}P{^{1}H} NMR δ 20.97 (s, μ-O$_2$P(O^{t}Bu)$_2$).

5b. Anal. Calcd for $C_{44}H_{102}N_2Mo_2N_2O_{16}P_2Si_2$ (%): C, 43.13; H, 8.39; N, 2.29. Found: C, 43.20; H, 8.50; N, 2.23. IR (cm^{-1}): 2974 vs, 2931 m, 2877 br w, 2778 w, 2725 w, 1473 w, 1389 w, 1365 m, 1246 m, 1194 s, 1134 w, 1117 w, 1057 vs, 984 s, 943 sh w, 916 w, 877 w, 827 w, 795 w, 754 w, 721 w, 700 w, 645 w, 602 w, 561 w, 498 w. ^{1}H NMR δ 5.19 (s, 6 H, NCH_3), 3.13 (s, 6 H, NCH_3), 1.69 (s, 18 H, μ-O$_2$P(O^{t}Bu)$_2$), 1.54 (s, 54 H, Si(O-^{t}Bu)$_3$), 1.45 (s, 18 H, μ-O$_2$P(O^{t}Bu)$_2$). ^{13}C{^{1}H} NMR δ 72.89 (s, Si(O*C*(CH$_3$)$_3$), 32.18 (s, Si(OC(*C*H$_3$)$_3$), 30.58 (d, μ-O$_2$P(OC(CH$_3$)$_3$, J = 4.0 Hz), 30.12 (d, μ-O$_2$P(OC(*C*H$_3$)$_3$, J = 4.6 Hz). No N*C*H$_3$ or μ-O$_2$P[O*C*(CH$_3$)$_2$]$_2$ resonances were observed. ^{31}P{^{1}H} NMR δ 22.95 (s, P, μ-O$_2$P(O^{t}Bu)$_2$).

$Mo_2(NMe_2)_2[\mu\text{-}O_2P(O^tBu)_2]_2\{OB[OSi(O^tBu)_3]_2\}_2$ (6). To a stirred pentane (10 mL) solution of **3** (0.305 g, 0.206 mmol) in a Schlenk tube was added (dropwise over 10 min) a pentane (10 mL) solution of $HOP(O)(O^tBu)_2$ (0.087 g, 0.413 mmol) at 25 °C. The dark red reaction mixture was stirred for an additional 10 min, concentrated to 2 mL, and cooled to −30 °C. Analytically pure purple crystals of **6** were isolated from two crops in 22% overall yield (0.083 g, 0.046 mmol) after washing with cold (−30 °C) pentane. Anal. Calcd for $C_{68}H_{156}B_2Mo_2N_2O_{26}P_2Si_4$ (%): C, 45.23; H, 8.71; N, 1.55. Found: C, 45.16; H, 8.84; N, 1.51. IR (cm^{-1}): 2976 vs, 2932 m, 2908 m, 2874 w, 2823 w, 2774 w, 1474 m, 1458 m, 1419 m, 1389 s, 1365 vs, 1339 s, 1244 m, 1193 vs, 1058 vs, 1029 sh s, 915 w, 830 m, 701 s, 604 w, 527 m, 483 m, 429 w. ^{1}H NMR δ 5.78 (s, 6 H, NCH_3), 3.173 (s, 6 H, NCH_3), 1.57 (s, 54 H, Si(O^{t}Bu)$_3$), 1.56 (s,

36 H, μ-$O_2P(O^tBu)_2$). $^{13}C\{^1H\}$ NMR δ 72.53 (s, $Si(OC(CH_3)_3)$, 32.25 (s, $SiOC(CH_3)_3$), 30.60 (m, μ-$O_2P[OC(CH_3)_2]_2$). No NCH_3 or μ-$O_2P[OC(CH_3)_2]_2$ resonances were observed. $^{31}P\{^1H\}$ NMR δ 21.02 (s, P, μ-$O_2P(O^tBu)_2$).

Xerogel Formation from 4a, 5a, and 5b. Representative solution thermolyses were carried out as follows. A thick-walled Pyrex pyrolysis tube was charged with a toluene (1 mL per 0.1 mmol of precursor) solution of either **4a** (0.300 g, 0.269 mmol), **5a** (0.250 g, 0.204 mmol), or **5b** (0.250 g, 0.204 mmol) in a glovebox (N_2 atmosphere). The tube was flame-sealed after three freeze−pump−thaw cycles and placed in a preheated oven at 150 °C for ∼90 h. A dark brown monolithic gel was formed, in all cases, after heating for 24 h. The tube was cooled to room temperature, opened, and the gel was quickly transferred to a Schlenk tube under N_2. The gel was then dried under a flow of N_2 for ∼72 h, subsequently dried in vacuo for 24 h at 120 °C, and stored under N_2 in a glovebox. The following xerogels were formed from **4a**, **5a**, and **5b**, respectively: **MoOP$_{xg}$**, 0.165 g (55.1% ceramic yield); ***t*-MoOPOSi$_{xg}$**, 0.131 g (52.5% ceramic yield); and ***c*-MoOPOSi$_{xg}$**, 0.130 g (52.0% ceramic yield). Calcinations of the xerogels were carried out in a Lindberg 1200 °C three-zone tube furnace under O_2 (100 mL min^{-1}). The heating rate was 10 °C min^{-1} and the final temperature was maintained for 2 h. All materials were heated at 120 °C for 24 h in vacuo and were subsequently stored under N_2 after each calcination stage.

Xerogel Formation from 4a and Bi[OSi(O^{t}Bu)$_3$]$_3$. Solution thermolyses were carried out as described above for the single-component experiments, except that amounts of **4a** and $Bi[OSi(O^tBu)_3]_3$ were used such that the total concentration was 0.10 mmol per mL of toluene. In all cases, monolithic gels were obtained. Materials with Bi/Mo/P/Si ratios of 1:1:2:3, 2:1:2:6, and 4:1:1:12 (corresponding to 2:1 (**BiMoPSi$_{2:1}$**), 4:1 (**BiMoPSi$_{4:1}$**), and 8:1 (**BiMoPSi$_{8:1}$**) $Bi[OSi(O^tBu)_3]_3$/**4a**) were synthesized. Postsynthesis treatments were as above for **MoOP$_{xg}$**.

Oxidative Dehydration of Propane. Selectivities and conversions for the propane ODH reactions were measured using a fixed-bed flow reactor (quartz) fitted with a medium frit. Quartz chips (0.500 g, 0.246−0.494 mm) were used to disperse each catalyst within the reactor. The mass of catalyst used varied between 0.010 and 0.030 g. Each catalyst was calcined at 500 °C under He/O_2 (10:1) for 2 h prior to reaction. The gas stream during catalytic reactions consisted of helium (typically 200 mL min^{-1}), propane (25 mL min^{-1}), nitrogen (2 mL min^{-1}), and oxygen (9 mL min^{-1}). Propane and oxygen conversions were varied by changing the total flow rate (between 40 and 240 mL min^{-1}). The gaseous reactants and products were analyzed online using a Hewlett-Packard 6890 gas chromatograph equipped with both a capillary column (HP-1) and a packed column (HAYESEP-Q), with C_3H_6, CO, CO_2, and H_2O as the only detected reaction products. The ODH reactions were run at 450 or 500 °C. Typical propane conversions for **MoOP$_{xg}$** ranged from ∼0.02 to 1%, with oxygen conversions from ∼0.8 to 6% at 450 °C. For the **BiMoPSi** materials, propane conversion ranged from ∼0.02 to 2%, with oxygen conversions from ∼0.04 to 2% at 500 °C.

Acknowledgment. This work was supported by the Director, Office of Energy Research, Office of Basic Energy Sciences, Chemical Sciences Division, of the U. S. Department of Energy under Contract DE-AC03-76SF00098. We thank A. Stacy (UC Berkeley) for the use of instrumentation (DRUV-vis and PXRD) and P. Yu (UC Davis) for the MAS NMR spectra.

Supporting Information Available: Crystallographic information files (cif) and details of the crystallographic analyses for **1**−**6** (experimental details, crystallographic data, and selected bond distances and angles; pdf). This material is available free of charge via the Internet at http://pubs.acs.org.

CM030563K